Copy 228
RM L52A14

TECH LIBRARY KAFB, NM

NACA

RESEARCH MEMORANDUM

PRELIMINARY INVESTIGATION OF THE DRAG CHARACTERISTICS OF

THE NACA RM-10 MISSILE AT MACH NUMBERS OF 1.40

AND 1.59 IN THE LANGLEY 4- BY 4-FOOT

SUPERSONIC TUNNEL

By Lowell E. Hasel, Archibald R. Sinclair,
and Clyde V. Hamilton

Langley Aeronautical Laboratory
Langley Field, Va.

NATIONAL ADVISORY COMMITTEE
FOR AERONAUTICS
WASHINGTON
April 18, 1952

PERMANENT

Classification cancelled (or changed to..Unclassified...........)

By Authority of   NASA Technical Announcement

(OFFICER AUTHORIZED TO CHANGE)   74 30 NOV 54

By.............. ......
NAME

GRADE OF OFFICER MAKING CHANGE)

.............)0 Apr 62)........
DATE

NATIONAL ADVISORY COMMITTEE FOR AERONAUTICS

RESEARCH MEMORANDUM

PRELIMINARY INVESTIGATION OF THE DRAG CHARACTERISTICS OF

THE NACA RM-10 MISSILE AT MACH NUMBERS OF 1.40

AND 1.59 IN THE LANGLEY 4- BY 4-FOOT

SUPERSONIC TUNNEL

By Lowell E. Hasel, Archibald R. Sinclair,
and Clyde V. Hamilton

SUMMARY

A parabolic body of revolution (0.287-scale model of the NACA RM-10) has been tested in the Langley 4- by 4-foot supersonic tunnel at Mach numbers of 1.40 and 1.59, and at Reynolds numbers based on body length varying from 1.8×10^6 to 4.7×10^6. The effects of Reynolds number, fins, internal contour of body base, and two support systems on body pressure and force drag were investigated at an angle of attack of 0°.

Laminar flow existed over the entire length of the sting-supported body (without fins). Addition of a transition strip at the maximum body diameter produced turbulent flow over the rear part of the body but did not significantly affect the forebody pressure distribution. The base pressure, however, was more negative than that produced by a corresponding laminar flow. When the fins were added to the body the base pressure became more negative than on the body without fins and was independent of the type of boundary layer existing ahead of the fins. Fin interference effects on the forebody pressure drag were small.

Varying the internal contour of the model base had no significant effect on the base pressure.

The use of a central wire-support system extending ahead of the body produced a turbulent flow over the entire body but did not significantly affect the forebody pressure distribution.

INTRODUCTION

In an attempt to evaluate scale effect on slender bodies, the National Advisory Committee for Aeronautics has undertaken a coordinated research program to test a parabolic body of revolution having a fineness ratio of 12.2 (NACA RM-10 missile). Various scale models of this missile have been tested in NACA supersonic wind tunnels (references 1 to 4) and rocket-propelled models have been tested in flight (references 5 to 7). The data obtained in these tests cover a wide range of Reynolds numbers and, at a given Mach number, data are available for a range of Reynolds number. In general, this attempt to evaluate the scale effect has been limited to the analysis of the drag coefficient at an angle of attack of 0°.

This paper presents a preliminary investigation of the drag characteristics which were obtained in the Langley 4- by 4-foot supersonic tunnel from a 0.287-scale model of the RM-10. The tests were made at Mach numbers of 1.40 and 1.59 and cover a Reynolds number range from 1.8×10^6 to 4.7×10^6. In addition to determining the zero-lift drag, the following factors were investigated: effect of two support systems on the pressure and force results, effect of base contour on the base pressure, fin-drag and fin-interference effects, and angle-of-attack effects.

SYMBOLS

A	maximum cross-section area of body
A_l	surface area of body with laminar boundary-layer run
A_W	total surface area of body forward of base
a	speed of sound in air
C_D	drag coefficient (D/qA)
D	drag
D_{max}	maximum model diameter

D_S　　　　　sting or windshield diameter

L　　　　　length of model

l　　　　　length of laminar boundary-layer run on model

M　　　　　Mach number　(V/a)

P　　　　　pressure coefficient　$\left(\dfrac{p_l - p}{q}\right)$

p　　　　　free-stream static pressure

p_l　　　　　local static pressure

q　　　　　dynamic pressure　$\left(\dfrac{\gamma}{2}\, pM^2\right)$

R　　　　　Reynolds number　$\left(\dfrac{\rho V L}{\mu}\right)$

R_l　　　　　Reynolds number based on length of laminar boundary-layer run　$\left(\dfrac{\rho V l}{\mu}\right)$

V　　　　　free-stream velocity

u　　　　　local stream velocity in boundary layer

x　　　　　axial distance from model nose

α　　　　　angle of attack

γ　　　　　ratio of specific heats of air

θ　　　　　model boattail angle

μ　　　　　viscosity

ρ　　　　　free-stream density

Drag-coefficient subscripts:

B　　　　　base drag

F　　　　　fore drag

f   skin-friction drag

p   fore pressure drag

T   total drag

W   total-drag increment per fin

w   fore-drag increment per fin

APPARATUS

Tunnel and Test Equipment

The Langley 4- by 4-foot supersonic tunnel is a single-return, closed-throat tunnel (see fig. 1, reference 8) driven at the time of these tests by a 6000-horsepower electric-drive system coupled to an axial-flow compressor. The maximum stagnation pressure was limited by the available drive power to about 0.3 atmosphere. (The tunnel power has since been increased to 45,000 horsepower). The design Mach number variation is from 1.2 to 2.2. Fixed parallel side walls and flexible top and bottom walls extend from a point 66 inches upstream of the first minimum section to the end of the test section, a total length of 25 feet. The test section is approximately 4.4 feet high and 4.5 feet wide. An activated-alumina air-drying system is used to maintain the stagnation dew point at a temperature where condensation effects are negligible.

Stagnation, free-stream, and model pressures were photographically recorded on multiple-tube manometers filled with Alkazene 42 (x-dibromoethylbenzene). This liquid has a specific gravity of approximately 1.75. The force data were obtained from a strain-gage balance and were visually recorded from a Brown self-balancing potentiometer. The strain gages were temperature compensated. Schlieren pictures were taken of several test configurations. Because of the low test-section density (0.03 to 0.09 atmosphere static pressure), however, few flow details were visible.

MODELS AND SUPPORT SYSTEMS

General model configuration.- The basic shape of the RM-10 body is generated by revolving a parabolic arc about a chord to form a body having a fineness ratio of 15. In order to facilitate installation of rocket motors in the rocket-propelled test vehicles the rearward 18.6 percent of the theoretical body was removed so that the actual

fineness ratio of the missile is only 12.2. Four stabilizing fins having a 10-percent-thick circular-arc section perpendicular to the leading edge are attached at the rear of the body. These fins have a 60° sweptback leading edge and no taper. Each fin has a half span of approximately 12.2 percent of the missile length. The length of the 0.287-scale model tested in the Langley 4- by 4-foot supersonic tunnel is 42.05 inches. Other pertinent dimensions are given in figure 1.

Model construction.- The model was constructed so that its weight was kept at a minimum so that the sag of the wire-support system would be small. A short nose section approximately four inches long and interchangeable base sections approximately eight inches long were constructed of magnesium. The remaining midsection of the body was formed by glueing a $\frac{1}{4}$-inch-thick layer of balsa wood around a load-carrying structure consisting of four longitudinal magnesium tubes. Glass fiber cloth was then wrapped around the balsa wood and impregnated with a thermosetting plastic. This plastic surface was stable, readily machined, and hard enough to withstand accidental marring encountered during the test program. The four model fins were machined from magnesium. The total weight of the model including the four fins and internal strain-gage assembly was approximately 4.6 pounds.

Nose section.- The nose details of the model are shown in figure 2(a). Clearance at the nose for the wire support was provided as shown in figure 2(a) by removing approximately three-fourths of an inch of the pointed tip. The remaining blunt nose was 0.25 inch in diameter. A $\frac{3}{16}$-inch-diameter hole was drilled through this blunt nose to provide clearance for the support wire. During most of the tests, the body shape was continued ahead of the blunt nose by means of conical wooden fairings which were glued to the wire. A second nose section was used during some of the preliminary tests. This section, which was tight fitting on the wire, continued the body contour until the body diameter was the same as that of the wire; thereby the need for a conical fairing was eliminated. Orifices were installed in both nose sections to measure the pressure distributions.

Base sections.- The four interchangeable bases used with the model are shown in figures 2(b) to 2(e). These bases attached to the body 34.05 inches from the pointed nose. The rocket, recessed, and flat bases were of identical external shape. The internal base contours were varied, however, as illustrated. Each of these bases was provided with an end plate through which a $\frac{1}{4}$-inch-diameter hole was drilled to provide clearance for the support wire. Each base contained a number of orifices for the determination of the base pressure and the external pressure

distribution. Similar bases were constructed for mounting from one to four fins with 90° spacings or from one to three fins with 120° spacings. The pointed base (fig. 2(e)) when attached to the fore section of the body formed the basic body of revolution from which the RM-10 body was derived. Orifices were located along this base to measure the external pressure distribution.

Support system.- The general arrangement of the wire-support system is shown in figure 3. A $\frac{1}{8}$ - inch-diameter wire approximately 35 feet long extended along the tunnel center line from the settling chamber through the supersonic nozzle to the end of the test section. The wire was anchored at its upstream end by four streamlined guy wires extending diagonally to the corners of the square settling chamber. The downstream anchorage was attached to the permanent model-support strut and included a wire loading device by which an initial preload of 1200 pounds tension was put in the wire to reduce the sag. Model misalinement caused by the sag which remained in the wire after the preload was applied was removed by positioning the upstream wire anchorage above the tunnel center line.

The internal strain-gage beam balance arrangement is shown in figure 1. Two beams located approximately as shown in figure 1 supported two ball bearings which in turn supported the model. This arrangement left the model free to rotate and prevented the wire from being over-stressed by inadvertent torsional loads due to fin misalinement or stream irregularities. A small control surface was provided on one fin to control the rate of roll of the model. The rate of roll, however, was so small (maximum tip helix angle was 0.14°) that the control surface was never used.

Figure 4 is a photograph of the wire-supported model with the rocket base. The method of bringing the strain-gage leads and pressure leads out the rear of the model is illustrated in this figure.

Sting-Supported Force Model

Only a few modifications to the nose and base of the wire-supported model were required to adapt it to a conventional sting support. A conical wooden fairing was placed in the blunt nose of the wire-supported model to form the pointed tip of the body. The end plates of the bases shown in figures 2(b) and 2(d) were drilled out to approximately $\frac{7}{8}$ - inch diameter to accommodate the 0.75-inch-diameter sting. (The ratio of sting to base diameter is 0.36.) The rocket nozzle contour of the rocket base was modified to permit attachment of the sting to the internal balance. A photograph of the sting-supported model is shown in figure 5.

Sting-Supported Pressure Model

The pressure model (fig. 6) was constructed of steel and had approximately 140 orifices located in four longitudinal rows 90° apart. The sting support was 1.25 inches in diameter (the ratio of sting to base diameter is 0.60). The pressure tubes connecting the orifices to the manometers were brought out through the interior of the sting as seen in figure 6. The model was tested both with a pointed-nose and with a faired-nose section similar to that shown in figure 2(a) which included a dummy wire support extending from the nose of the model to the upstream support anchorage.

TESTS, CORRECTIONS, AND ACCURACY

Tests

The following table summarizes the variable test conditions. The complete test program is tabulated in tables I and II.

Model	Mach number	Average Reynolds number	Angle of attack (deg)
Wire-supported model	1.59	1.8×10^6 to 4.7×10^6	0
Sting-supported force model	1.59	2.7×10^6 to 4.5×10^6	0 to 6
Sting-supported force model	1.40	3.8×10^6	0
Sting-supported pressure model	1.59	3.7×10^6	0
Sting-supported pressure model with dummy wire support	1.59	2.8×10^6 to 4.7×10^6	0

All tests were conducted with a stagnation temperature of 110° F. The stagnation dew point was kept more negative than -35° F at $M = 1.59$ and more negative than -25° F at $M = 1.40$.

Evaluation of wire-support system.- Prior to any systematic model testing a series of tests were made at a Mach number of 1.59 and a Reynolds number of 3.7×10^6 to measure the thickness of the support-wire boundary layer and to evaluate the effects of the wire-support system on the model pressure distribution. The effects of both detail model design and internal air flow on the nose and base pressure distributions were also determined. These tests are tabulated in table I.

Basic tests.- The initial tests of the main test program were made to determine the effect of air-stream irregularities on the drag data. In making this study, the model was located at four positions along the longitudinal center line of the tunnel. (Nose locations were at stations 239, 230, 222, and 215 for the reference system of reference 8 and fig. 3 of this paper.) During the remainder of the tests, the model nose was located at station 215 since this position represented the upstream limit of the stream surveys and also minimized the effect of the wire loading device on the model base pressure.

Drag data were obtained at $M = 1.59$ on the wire-supported model with the flat, recessed, rocket, and pointed bases. The effect of locating a transition strip formed by a thin layer of number 60 carborundum $\frac{1}{4}$-inch wide at several body locations was determined, and the incremental drag of the fins was measured. At Mach numbers of 1.40 and 1.59, the sting-supported force model with the rocket and flat bases was used to obtain the body fore drag, base drag, and fin drag. The effect on these drag characteristics of locating a transition strip on the body at $\frac{X}{L} = 0.614$ was determined. At a Mach number of 1.40 the fin interference on the fuselage pressure distribution was also determined. These tests are tabulated in table II.

Base-pressure and drag-force data were obtained simultaneously from the sting-supported force model. Previous tests showed that a static orifice located on the sting near the end of the rocket base indicated the same base pressure as those orifices located on the base itself. Since the sting-mounted orifice was not directly connected to the model, no tare forces were introduced by using it to obtain base pressure during the force tests.

Corrections and Accuracy

The variations of free-stream Mach number and flow angle on the tunnel center line in the region of the model at a Mach number of 1.59 are summarized in the following table.

Mach number variation	0.015 -.005
Horizontal flow angle variation	-0.25 .00
Vertical flow angle variation	-0.30 .15

Corrections have been applied to the pressure data to account for the free-stream pressure distribution which is given in figure 6 of reference 8. The corrections were made by subtracting the local-stream static-pressure distribution from the measured pressures. The force results have also been corrected for the corresponding buoyancy force. No corrections have been made to the Mach number 1.40 data because of insufficient information concerning the free-stream distribution in the test section. The corrections, however, are believed to be of the same magnitude as those applied at a Mach number of 1.59.

The accuracy of the body shape was determined by measuring the force model diameter at 1-inch intervals along the body. The results of these measurements are presented in table III as the difference between the measured and computed diameter at each station. The maximum disagreement is 0.007 and -0.014 inch. No corrections to the data have been made for these discrepancies.

The accuracy of the pressure coefficient and drag coefficient is estimated to be as follows:

M	R	P	Fore and base drag coefficient
1.59	1.8×10^6	±0.015	±0.006
1.59	2.7×10^6	±.012	±.005
1.59	3.7×10^6	±.010	±.004
1.59	$\begin{cases} 4.5 \times 10^6 \\ 4.7 \times 10^6 \end{cases}$	±.009	±.003
1.40	3.8×10^6	±.012	±.003

PRESENTATION AND DISCUSSION OF RESULTS

Evaluation of Wire-Support System

Wire boundary layer.- The boundary-layer velocity profiles on the support wire at station 215 were computed from total-pressure surveys and are shown in figure 7. In reducing the data the assumption was made that the static pressure and stagnation temperature were constant throughout the boundary layer. The boundary-layer profile at the end of the 27.5-foot run on the wire has turbulent boundary-layer characteristics. On the top of the wire (tailed symbols) the boundary-layer velocity reaches 99 percent of the free-stream value 1.4 inches from the wire surface. On the bottom of the wire the corresponding distance is 0.9 inch. This difference in thickness occurs because the support wire slopes upward slightly from the test section to the settling chamber.

Effect of wire boundary layer on body pressure distribution.- The effect of the wire boundary layer on the pressure distribution over the body is shown in figure 8 where the pressure distributions obtained on the pressure model with and without the dummy wire support are presented. Each data point in this figure was obtained by averaging the data from four orifices spaced 90° apart. (The spread between the individual orifice pressures was small.) It is apparent that over all of the body, except the rearmost five percent, the wire boundary layer has no significant effect on the pressure distribution. The experimental results are in good agreement with the linear-theory results computed by the method presented in reference 9. Integration of the pressure distributions to obtain the forebody pressure drag coefficient based on the maximum frontal area gives the following results.

Source	c_{D_p}
Linear theory	0.047
Sting-supported model	.041
Sting-supported model with dummy wire support	.044

The base pressure changes from -0.015 to -0.082 when the dummy wire support is added to the model configuration. As is shown later, this change in base pressure is caused by a change in boundary-layer flow conditions existing at the body base on these two configurations.

Data obtained on the wire-supported body with the pointed base substantiate the above reasoning concerning the change of base pressure. On the latter body where there is no abrupt change of body shape at $\frac{x}{L} = 1.0$, the pressure distribution (fig. 9) has no tendency suddenly to become more negative at this point. Instead there appears to be a pressure recovery over the rear of the body which is in good agreement with linear theory. The experimental forebody pressure drag coefficient of this complete body of revolution is 0.044. The total drag coefficient is 0.164.

It is possible to compare the present results with those of reference 10 and to obtain the reason for the large observed shift in base pressures. In reference 10, the results of a study at a Mach number of 1.5 of the effects of viscosity on the drag of bodies of revolution are presented. Several bodies (models 4 and 5) the shapes of which are mathematically similar to the RM-10 body shape were among those tested. The base pressure coefficients measured on these bodies and on the RM-10 body are presented in figure 10 as a function of the boattail angle θ[1]. It can be seen that the RM-10 data follow the trends established by the data from reference 10. This comparison indicates that the conventional sting-supported model probably has a laminar boundary layer over most of the body (a fact which will be indicated more tangibly later) and that turbulent flow exists over the rear part of the wire-supported body.

Effect of model construction details on nose pressure distribution.- In figure 11 the nose pressure distributions obtained with the faired (see fig. 2(a)) and tight fitting noses are shown. Pressure data were taken at two radial positions 180° apart and are distinguished by the two symbols. A comparison of the data in figures 11(a) and 11(b) indicates that the use of the faired nose with the conical fairing attached to the wire has no adverse effects on the nose pressure distribution. Furthermore, any air which may flow from the nose to the base of the body through its interior does not affect the external nose pressure distribution. The pressures obtained from these tests appear to be slightly more negative than those obtained from the sting-supported pressure model with the dummy wire support.

---

[1]For a general series of bodies the base pressure coefficient is a function not only of θ, but also of the surface Mach number near the body base, type of boundary layer, and the ratio of the boundary-layer thickness at the body base to the diameter of the body base (see reference 11). For the three bodies considered, however, the surface Mach number near the base is approximately constant as determined by linear theory, and the ratio of the boundary-layer thickness to the base diameter should also be about the same for each boundary-layer condition. When the sting interference effects are neglected, therefore, θ is the primary variable affecting the base pressure on these bodies.

These evaluation tests indicate that the wire-support system has little effect on the forebody pressure distribution of the RM-10. A similar general conclusion pertaining to all bodies, however, can not be made. The turbulent flow created by the wire support masks any effects of laminar separation which might exist on a conventional sting-supported model. On the RM-10 body these effects are small since a favorable pressure gradient exists over most of the model.

Effect of model construction details on base pressures.- In figure 12, the base pressures measured on the internal contours of the rocket and recessed bases are shown. At some of the orifice stations, four pressures 90° apart were obtained. These pressures are distinguished by use of different symbols. The average end-plate pressure of the two bases appears to be about the same.

On each base, however, there is a small variation of pressure within the base. These latter results are in agreement with the results of free-flight tests on a body of somewhat similar shape, reference 12, in which the base pressure measured on the center of the nozzle end plate was more positive than that measured nearer the exit of the nozzle. Furthermore, air flow through the model interior did not appreciably affect the base pressures.

Force Tests of Body Alone

The drag characteristics of the body alone are presented in figures 13 and 14. In figure 13 the total body drag, base drag, and forebody drag coefficients of the wire and sting-supported models are plotted as a function of Reynolds number. In figure 14, the forebody skin-friction drag coefficients are plotted as a function of Reynolds number and are compared with computed results.

Preliminary tests.- Prior to the basic force tests of the body alone, the effect of model location in the test section on the total drag characteristics of the body alone were determined. The following table summarizes the total-drag data obtained from the body fitted with the flat base when the model was located at four positions in the test section.

Station of nose location	C_{D_T} uncorrected	C_{D_T} corrected for buoyancy
239	0.190	0.182
230	.183	.181
222	.176	.181
215	.173	.180

An inspection of the data indicates that the application of the buoyancy correction reduced the drag-coefficient variation from 0.017 for the uncorrected results to 0.002 for the corrected results.

Total drag.- The total body drag coefficients of the wire-supported model at M = 1.59 (fig. 13(a)) vary from an average value of 0.197 at a Reynolds number of 1.8×10^6 to 0.172 at a Reynolds number of 4.7×10^6. All three of the bases give approximately the same value of drag coefficient.

The data obtained at a Mach number of 1.59 on the sting-supported model (fig. 13(b)) indicate the large effect which the boundary layer has on the total body drag coefficient. With a transition strip at $\frac{x}{L} = 0.614$, the drag coefficients vary from 0.153 at a Reynolds number of 2.8×10^6 to 0.146 at a Reynolds number of 4.5×10^6. Corresponding drag-coefficient values without a transition strip on the model are 0.079 and 0.093. At a Mach number of 1.40 and a Reynolds number of 3.8×10^6 the data obtained from the sting-supported model (fig. 13(c)) show the same trends as the corresponding data at a Mach number of 1.59. The effect of the transition strip, however, appears to be smaller at the lower Mach number. The total drag coefficients measured on the wire-supported model are about 20 percent higher than those measured on the sting-supported model with the transition strip located at $\frac{x}{L} = 0.614$.

Base drag.- Only two values of base drag coefficient (fig. 13(a)) were determined during the force tests on the wire-supported model. The average value of 0.025 obtained from these tests is in good agreement with the results of the preliminary tests (fig. 12) where the base drag coefficient based on end-plate pressure (-0.07) is 0.026. On the sting-supported model the base-drag coefficients are higher with turbulent flow over the rear of the model and change very little with increasing Reynolds number in contrast to the increase in base drag coefficient with increasing Reynolds number on the model with no transition strip. Over the small Mach number range of these tests there appear to be no Mach number effects on the base drag coefficient of the sting-supported model.

The base drag coefficients obtained from the two force models and the pressure model are summarized in the following table for a Reynolds number of 3.7×10^6 and a Mach number of 1.59. Since the sting configuration may influence the base drag coefficient the sting dimensions are also included in the table.

Model	Boundary-layer condition at model base	Sting diameter (in.)	Length of straight sting behind model (in.)	Base drag coefficient
Wire-supported force model	Turbulent	0.125	Greater than 20	0.025
Wire-supported force model with dummy sting	Turbulent	1.25	8	.028
Sting-supported force model	Turbulent	0.75	8	.035
Sting-supported pressure model	Turbulent	1.25	4	.030
Sting-supported force model	Laminar	0.75	8	.017
Sting-supported force model with larger diameter dummy sting	Laminar	1.25	10.5	.007
Sting-supported pressure model	Laminar	1.25	4	.006

A comparison of the values in this table is rather difficult because of the possibility of sting-interference effects being present. On the configurations with turbulent flow over the rear of the models the base drag coefficient varied from 0.025 to 0.035. The base drag coefficient is lowest on the wire-supported model which has the least probable sting interference effects. In this connection, a test was made to determine the magnitude of the sting-interference effects. When a dummy wooden sting 1.25 inches in diameter and 8 inches long (followed by a 20° included angle cone) was attached to the wire, the base drag coefficient was increased to 0.028; thus very little sting interference is indicated. The higher base drag coefficient of the sting-supported force model with partially turbulent flow may be due to a different thickness of the boundary layer at the model base (reference 11). With a laminar boundary layer over the rear of the model the base drag coefficients of the pressure and force models are 0.006 and 0.017, respectively. In a supplementary test the diameter of the force-model sting was increased to 1.25 inches to correspond to the pressure model. Under these conditions the measured base drag coefficient was 0.007 and indicates that with a

laminar boundary layer the larger sting does affect the base drag coefficient. No tests were made to determine whether the smaller sting also affected the base drag coefficient.

It should be noted that, in reference 11, the base pressure on a body with a boattail angle of 0° and with laminar boundary-layer flow became more negative as the sting diameter was increased. Reference 13, however, presents tests on a boattailed body with laminar flow in which the base pressure became more positive as the sting diameter was increased. It appears, therefore, that the effect of sting interference on base pressure is a function of body boattail angle.

Forebody drag.- The forebody drag coefficients presented in figure 13 were obtained by subtracting the base drag coefficients from the total body drag coefficients. Since the effect of Reynolds number on the base drag coefficients of the wire-supported model was not determined, the forebody drag coefficients were obtained by using the base drag coefficient measured at a Reynolds number of 3.7×10^6. Both the wire- and sting-supported model forebody drag data decrease with increasing Reynolds number. The forebody drag coefficients of the wire-supported model where the boundary layer is completely turbulent[1] are about 50 and 130 percent greater than corresponding values for the sting-supported model with and without a transition strip at the maximum diameter station. The data at a Mach number of 1.40 show much less effect due to the addition of the transition strip than the Mach number 1.59 data.

Skin-friction drag.- The forebody skin-friction drag coefficients presented in figure 14 for a Mach number of 1.59 were obtained by subtracting from the forebody drag coefficients (fig. 13) the pressure drag coefficient obtained from tests on the pressure model. The following table lists the pressure drag coefficients which were used.

	R	c_{D_p}
Wire-supported model	2.8×10^6	0.048
	3.7×10^6	.044
	4.7×10^6	.043
Sting-supported model	3.7×10^6	.041

[1]It will be shown later that the boundary-layer flow on the wire-supported model is completely turbulent.

Since pressure data for the sting-supported model were available only at a Reynolds number of 3.7×10^6, the pressure drag coefficient obtained at this Reynolds number was used for reducing all the skin-friction drag-coefficient data (fig. 14) for the sting-supported model. The data indicate that the sting-supported model with the laminar boundary layer has the lowest skin-friction drag. Addition of the transition strip more than doubles the skin-friction drag of this model, while use of the wire-support system more than triples the skin-friction drag over that of a laminar boundary layer. When the assumption is made that the transition strip causes boundary-layer transition it appears from the data that on the wire-supported model the boundary layer becomes turbulent over the forward part of the model. These data are substantiated by supplementary tests which were made on the wire-supported model in which the transition strip was located at different stations on the body. These data are summarized in the following table which shows the effect on the total drag coefficient of placing the transition strip at several locations $\frac{x}{L}$ on the model.

R	Transition-strip location				
	No transition strip	0.832	0.614	0.352	0.093
	c_{D_T}				
2.7×10^6	0.187	0.187	0.185	0.185	0.186 .189
3.7×10^6	.181	.179	.179	.178	.180
4.7×10^6	.173	.174	.174	.174	.174

For each Reynolds number, the total drag is the same, within the experimental accuracy of the data, regardless of the location of the transition strip. These results would be expected only if the boundary layer were already turbulent at the most forward location of the transition strip. It thus appears that on the wire-supported model the boundary layer is completely turbulent.

Computed skin-friction drag coefficients based on compressible-flow theory are also presented in figure 14. The evaluation of the skin-friction coefficient on bodies of revolution, when the effects of pressure gradient are neglected, has been discussed in reference 14. Further analysis, based on reference 14, of this problem has been performed by Mr. Clinton E. Brown of the Langley Laboratory. It can be

shown from the unpublished analysis that, with laminar flow, the three-dimensional skin-friction coefficient for the RM-10 body (pressure gradient effects being neglected) is about 6 percent greater than the equivalent flat-plate skin-friction coefficient which can be obtained from an empirical equation

$$c_f \sqrt{R} = 1.328 - 0.0217 M^{1.5} \tag{1}$$

presented in reference 15. (Equation (1) is a good approximation to the results presented in references 16 and 17.) The computed laminar skin-friction drag coefficients in figure 14 were therefore computed from the equation

$$C_{D_f} = \frac{1.06}{\sqrt{R}} \left(1.328 - 0.0217 M^{1.5} \right) \frac{A_w}{A} \tag{2}$$

Mr. Brown has also shown that, for practical bodies of revolution, the percentage difference between the three-dimensional and equivalent flat-plate turbulent-skin-friction coefficients is small and is probably within the accuracy of the analysis. The computed turbulent-skin-friction drag coefficients presented in figure 14, therefore, are obtained from the equation

$$C_{D_f} = \frac{0.472}{\left(\log_{10} R \right)^{2.58} \left(1 + \frac{\gamma - 1}{2} M^2 \right)^{0.467}} \frac{A_w}{A} \tag{3}$$

which is based on flat-plate results presented in reference 18.

As a matter of general interest, equations (2) and (3) have been combined to give the following equation for computing the skin-friction drag of a partially turbulent boundary layer

$$C_{D_f} = 1.06 \frac{\left(1.328 - 0.0217 M^{1.5} \right)}{\sqrt{R \frac{l}{L}}} \frac{A_l}{A} +$$

$$\frac{0.472}{\left(1 + \frac{\gamma - 1}{2} M^2 \right)^{0.467}} \left(\frac{1}{\left(\log_{10} R \right)^{2.58}} \frac{A_w}{A} - \frac{1}{\left[\log_{10} \left(R \frac{l}{L} \right) \right]^{2.58}} \frac{A_l}{A} \right) \tag{4}$$

Equation (4) assumes, for lack of a better assumption, that the transition strip creates a turbulent boundary layer of the same thickness back of the strip as would exist if turbulent flow also existed over that part of the model ahead of the strip.

The experimental laminar skin-friction coefficients presented in figure 14 are in good agreement with the results computed from equation 2. It appears, therefore, that the effects of pressure gradient on the laminar skin-friction drag may be small. The data from the wire-supported model (completely turbulent flow) agree with the results computed from equation (3). No significance should be placed on this agreement, however, since the wire support creates a turbulent flow at the model nose which does not start from zero thickness. The Reynolds number based on body length, therefore, is a fictitious number, and the experimental skin-friction drag has little significance.

Force Tests of Body Plus Fins

The drag data obtained with various numbers of fins attached to the wire-supported model are shown in figure 15. The total drag coefficient and the total drag increment per fin obtained from the rocket, recessed, and flat base models are plotted as a function of Reynolds number. The total drag coefficient of the four-finned body is very nearly constant at each Reynolds number for the three bases and varies from about 0.290 at a Reynolds number of 2.7×10^6 to a value of 0.270 at a Reynolds number of 4.7×10^6. The total-drag-coefficient increment per fin appears to be very nearly independent of Reynolds number, internal base contour, number of fins, and radial spacing of the fins. This drag increment has an average value of about 0.025. It should be mentioned that this total drag increment includes any change in base pressure drag of the body alone due to the addition of the fins, and any change in forebody pressure drag due to fin interference.

The drag data which were obtained on the sting-supported model at Mach numbers of 1.59 and 1.40 are presented in figures 16 and 17, respectively. The total drag, base drag, and fore drag coefficients, and the fore drag coefficient increment per fin are plotted as a function of Reynolds number. These data were obtained both with transition free (figs. 16(a) and 17(a)) and with transition strip at $\frac{x}{L} = 0.614$ (figs. 16(b) and 17(b)).

With four fins attached to the body and with a laminar boundary layer, the total drag coefficient at a Mach number of 1.59 (fig. 16(a)) varies from 0.220 at a Reynolds number of 2.8×10^6 to 0.211 at a

Reynolds number of 4.5×10^6. The corresponding drag values with turbulent flow (fig. 16(b)) over the rear of the model appear to be independent of the small Reynolds number range of these tests and have an average value of 0.231.

Addition of the fins has a considerably larger effect in increasing the base drag coefficient of the model with laminar flow than on the model with partially turbulent flow. The amount of the base drag increase on the model with laminar flow appears to be a function of the number of fins attached to the body. It is interesting to note that for both boundary-layer configurations the base pressures on the four-finned models are nearly equal. This result suggests that, perhaps, the base pressure on fin-stabilized models of this type may be relatively independent of the type of boundary-layer flow existing ahead of the fins, but may be considerably influenced by the flow field created by the fins.

The average fore-drag-coefficient increments per fin for the model with and without a transition strip are 0.024 and 0.018, respectively. These experimental values are somewhat greater than the linear-theory pressure drag computed by the method of reference 19. It must be remembered, however, that the experimental values include the effects of skin friction and interference effects on the fuselage and between fins.

Corresponding drag data (fig. 17) were obtained at a Mach number of 1.40 for a Reynolds number of 3.8×10^6. These data show no significant differences from that obtained at a Mach number of 1.59. The total drag coefficients of the four-finned model at the lower Mach number are 0.227 (laminar flow) and 0.242 (partially turbulent flow) as compared to comparable values of 0.212 and 0.234 at a Mach number of 1.59. This decrease with Mach number of the total drag coefficient is due to a decreasing fore drag coefficient since the base drag coefficients are about the same at both Mach numbers.

Force Tests of Body Alone at Angles of Attack

A small amount of angle-of-attack data was obtained from the sting-supported body at a Mach number of 1.59 and a Reynolds number of 3.7×10^6. These data are presented in figure 18 where the total, base, and fore drag coefficients are presented as a function of angle of attack. Similar data obtained on a half-scale model at a Reynolds number of 29.2×10^6 in the Lewis 8- by 6-foot supersonic tunnel (reference 2) are also presented. The base-drag-coefficient results from reference 2 were obtained by averaging the values obtained with increasing and decreasing angles of attack. The total drag coefficient of the body with laminar flow increases more rapidly with angle of attack than does the total drag of the body with attached transition strip. This relative variation appears

to be partly caused by the behavior of the base drag on the laminar-flow model. It would appear from these data that the base-drag variation on a model with laminar flow is larger at small angles of attack than on a model with turbulent flow. Qualitatively, the data obtained with the transition strip on the model follow the same trends as the Lewis data.

Fin Interference

The fin-interference effects on the fuselage pressure distribution are shown in figure 19(a). In this figure, the pressure coefficients which were obtained on a $90°$ radial sector of the fuselage are plotted as a function of the orifice location. The tailed symbols are data obtained with a transition strip at $\frac{x}{L} = 0.614$; the untailed data were obtained with laminar flow over the fuselage. The fuselage pressure distribution obtained without fins is presented in figure 19(b). When figures 19(a) and 19(b) are compared it appears that, with a laminar boundary layer, the presence of the fins is felt about 5 percent of the body length or about 45 percent of the fin-chord length (measured parallel to the model axis) ahead of the fuselage-fin leading-edge juncture. At a given station the radial pressures are uniform and reach a maximum positive pressure approximately 50 percent of the fin-chord length behind the fuselage-fin leading-edge juncture. The pressures then decrease at a rapid rate until the base of the model is reached. With a turbulent flow the effect of the fins is apparently not propagated forward on the body nor is the pressure uniform at any radial station. Integration of these pressure results indicates that, with the laminar boundary layer, the interference effects of the fins on the body reduce the fore pressure drag coefficient by 0.007. The corresponding value for the turbulent boundary layer over the rear of the model is 0.008. It is probable that the fin-body juncture causes transition over the rear of the body.

General Correlation

Data of the complete model which were available from these and other investigations at a Mach number near 1.6 have been plotted as a function of Reynolds number in figure 20. The total drag coefficients vary from 0.211 to 0.254. When the transition-free data obtained in the 4- by 4-foot supersonic tunnel are assumed to be typical data at the low Reynolds numbers (this is verified by the data of the Langley 9-inch supersonic tunnel), the total drag varies about twenty percent over the Reynolds number range, and the base drag decreases slightly. As a result of the opposite trends of the total and base drags, the fore drag coefficient varies about 30 percent over the Reynolds number range.

In figure 21, the experimental skin-friction drag of the forebody without fins at a Mach number of 1.6 is plotted as a function of Reynolds number. The rocket-propelled flight data were obtained by subtracting from the forebody drag of the complete model the fin drag, as measured on a cylindrical body with no boattailing, and the theoretical forebody pressure drag. The data from the Langley 9-inch supersonic tunnel were obtained by subtracting from the forebody drag of the complete model the theoretical fin and forebody pressure drag and a computed laminar skin-friction fin drag based on theoretical flat-plate results. These data give an indication of the magnitude of the scale effects which may be expected on this type of model. At low Reynolds numbers where the boundary layer is laminar the skin-friction drag decreases as the Reynolds number increases. This trend is reversed at higher Reynolds numbers as the location of boundary-layer transition gradually moves forward on the body with increasing Reynolds number. The total variation of the skin-friction drag coefficient over the Reynolds number range of these tests cannot be determined since the Reynolds number at which transition begins is not known and the skin-friction drag coefficient continually decreases until this value of Reynolds number is reached. However, from the available data it appears that the maximum skin-friction drag coefficient (wire-supported model and fixed-transition data being neglected) may be at least 300 percent of the minimum value since this variation is present in the data of figure 20 and these data do not define the true maximum or minimum values.

The theoretical variations of the RM-10 skin-friction drag coefficient for laminar- and turbulent-compressible-boundary-layer flow are also presented in figure 21. These variations were determined from basic equations (2) and (3). When the laminar-flow data from the Langley 4- by 4-foot tunnel are considered, it appears that these data have about the same values as the theoretical values. The experimental variation with Reynolds number is somewhat less than that predicted by theory. A comparison of the theoretical turbulent-skin-friction drag coefficient may be made with the Pilotless Aircraft Research Division full-scale data since it is estimated on the basis of unpublished data that turbulent flow exists on about 97 percent of the body wetted area. This experimental value has about the same value as the theoretical value. The completely turbulent data obtained in the Langley 4- by 4-foot tunnel indicate good agreement with the theoretical result. It must be remembered, however, that the actual Reynolds number of the flow over this model is not known because of the initial wire boundary layer. Hence the good agreement may be coincidental.

CONCLUSIONS

A parabolic body of revolution (0.287-scale model of the NACA RM-10) has been tested in the Langley 4- by 4-foot supersonic pressure tunnel at Mach numbers of 1.40 and 1.59 and at Reynolds numbers based on body length varying from 1.8 to 4.7×10^6. The effects of Reynolds number, fins, internal contour of body base, and two support systems on the body pressure and force drag were investigated at an angle of attack of $0°$.

The following conclusions have been obtained:

(1) Laminar flow existed over the entire length of the sting-supported body (without fins). Addition of a transition strip at the maximum body diameter produced turbulent flow over the rear part of the body but did not significantly affect the forebody pressure distribution. The base pressure, however, was more negative than that produced by a corresponding laminar flow.

(2) The addition of fins resulted in a base pressure which was more negative than for the body without fins and which was independent of the type of boundary layer existing ahead of the fins.

(3) The effect of fin interference on the forebody pressure drag was small.

(4) The internal contour of the model base had no significant effect on the base pressure.

(5) The use of a central wire-support system extending ahead of the body produced a turbulent flow over the entire body but did not significantly affect the forebody pressure distribution.

Langley Aeronautical Laboratory
    National Advisory Committee for Aeronautics
        Langley Field, Va.

REFERENCES

1. Luidens, Roger W., and Simon, Paul C.: Aerodynamic Characteristics of NACA RM-10 Missile in 8- by 6-Foot Supersonic Wind Tunnel at Mach Numbers from 1.49 to 1.98. I - Presentation and Analysis of Pressure Measurements (Stabilizing Fins Removed). NACA RM E50D10, 1950.

2. Esenwein, Fred T., Obery, Leonard J., and Schueller, Carl F.: Aerodynamic Characteristics of NACA RM-10 Missile in 8- by 6-Foot Supersonic Wind Tunnel at Mach Numbers from 1.49 to 1.98. II - Presentation and Analysis of Force Measurements. NACA RM E50D28, 1950.

3. Luidens, Roger W., and Simon, Paul C.: Aerodynamic Characteristics of NACA RM-10 Missile in 8- by 6-Foot Supersonic Wind Tunnel at Mach Numbers from 1.49 to 1.98. III - Analysis of Force Distribution at Angle of Attack. NACA RM E50I19, 1950.

4. Allen, H. Julian, and Perkins, Edward W.: Characteristics of Flow over Inclined Bodies of Revolution. NACA RM A50L07, 1951.

5. Jackson, H. Herbert, Rumsey, Charles B., and Chauvin, Leo T.: Flight Measurements of Drag and Base Pressure of a Fin-Stabilized Parabolic Body of Revolution (NACA RM-10) at Different Reynolds Numbers and at Mach Numbers from 0.9 to 3.3. NACA RM L50G24, 1950.

6. Rumsey, Charles B., and Loposer, J. Dan: Average Skin-Friction Coefficients from Boundary-Layer Measurements in Flight on a Parabolic Body of Revolution (NACA RM-10) at Supersonic Speeds and at Large Reynolds Numbers. NACA RM L51B12, 1951.

7. Chauvin, Leo T., and deMoraes, Carlos A.: Correlation of Supersonic Convective Heat-Transfer Coefficients from Measurements of the Skin Friction Temperature of a Parabolic Body of Revolution (NACA RM-10). NACA RM L51A18, 1951.

8. Cooper, Morton, Smith, Norman F., and Kainer, Julian H.: A Pressure-Distribution Investigation of a Supersonic Aircraft Fuselage and Calibration of the Mach Number 1.59 Nozzle of the Langley 4- by 4-Foot Supersonic Tunnel. NACA RM L9E27a, 1949.

9. Lighthill, M. J.: Supersonic Flow Past Bodies of Revolution. R. & M. 2003, British A.R.C., 1945.

NACA RM L52A14

10. Chapman, Dean R., and Perkins, Edward W.: Experimental Investiga-
    tion of the Effects of Viscosity on the Drag of Bodies of Revolu-
    tion at a Mach Number of 1.5. NACA RM A7A31a, 1947.

11. Chapman, Dean R.: An Analysis of Base Pressure at Supersonic
    Velocities and Comparison with Experiment. NACA TN 2137, 1950.

12. Peck, R. F.: Flight Measurements of Base Pressure on Bodies of
    Revolution with and without Simulated Rocket Chambers. NACA
    RM L50I28a, 1950.

13. Perkins, Edward W.: Experimental Investigation of the Effects of
    Support Interference on the Drag of Bodies of Revolution at Mach
    Number of 1.5. NACA TN 2292, 1951.

14. Mangler, W.: Boundary Layers with Symmetrical Airflow about Bodies
    of Revolution. Rep. No. R-30-18, Part 20, Goodyear Aircraft Corp.,
    March 6, 1946.

15. Kuethe, Arnold M., and Epstein, Herman T.: Viscosity Effects in
    Transonic and Supersonic Flow, Bumblebee Rep. No. 48, Univ. Mich.,
    Dept Eng. Res., Dec. 1946.

16. Brainerd, J. G., and Emmons, H. W.: Effect of Variable Viscosity on
    Boundary Layers with a Discussion of Drag Measurements. Jour.
    Appl. Mech. (A.S.M.E.), vol. 9, 1942, p. A-1.

17. Von Kármán, Th., and Tsien, H. S.: Boundary Layer in Compressible
    Fluids. Jour. Aero. Sci., vol. 5, no. 6, April 1938, p. 227.

18. Rubesin, Morris W., Maydew, Randall C., and Varga, Steven A.: An
    Analytical and Experimental Investigation of the Skin Friction of
    the Turbulent Boundary Layer on a Flat Plate at Supersonic Speeds.
    NACA TN 2305, 1951.

19. Harmon, Sidney M., and Swanson, Margaret D.: Calculations of the
    Supersonic Wave Drag of Nonlifting Wings with Arbitrary Sweepback
    and Aspect Ratio. Wings Swept behind the Mach Lines. NACA
    TN 1319, 1947.

TABLE I.- SUMMARY OF TEST PROGRAM CONDUCTED ON THE RM-10 MODELS AT AN ANGLE OF ATTACK

OF 0° AT A MACH NUMBER OF 1.59 AND A REYNOLDS NUMBER OF 3.7×10^6

TO EVALUATE THE EFFECTS OF THE WIRE-SUPPORT SYSTEM

Model	Support configuration	Nose configuration	Nose location in tunnel (see fig. 3)	Base	Internal air flow through model	Pressure-distribution data obtained	Force data obtained	Base pressure measured
Pressure	Sting	Normal configuration	219	--------	No	Forebody and base	No	---
Pressure	Wire	Dummy wire support	219	--------	No	Forebody and base	No	---
Force	Wire	Faired	215	Recessed	Yes	Nose	No	No
Force	Wire	Faired	215	Recessed	No	Nose	No	No
Force	Wire	Tight fitting	215	Recessed	No	Nose	No	No
Force	Wire	Faired	215	Recessed	No	Base	No	Yes
Force	Wire	Faired	215	Recessed	Yes	Rearward forebody and base	No	Yes
Force	Wire	Faired	215	Rocket	Yes	Rearward forebody and base	No	Yes
Force	Wire	Faired	215	Pointed	Yes	Rearward forebody	No	No
Force	Wire	Faired	215	Pointed	Yes	No	Yes	No

CONFIDENTIAL

TABLE II.- SUMMARY OF BASIC TEST PROGRAM CONDUCTED ON RM-10 FORCE MODEL

Base configuration	M	R	α	Number of fins	Method of support	Transition strip at $\frac{x}{l} = 0.615$	Drag force data	Base pressure measured	Pressure-distribution tests	Nose configuration	Nose location in tunnel (see fig. 3)	Internal air flow through model
Flat	1.59	3.7×10^6	0	0	Wire	No	Yes	No	No	Faired	239	Yes
		3.7×10^6									230	
		3.7×10^6									222	
		3.7×10^6									215	
Recessed		3.7×10^6					No	Yes				
Rocket		3.7×10^6										
		1.8×10^6						Yes	No			
		2.7×10^6										
		3.7×10^6										
		4.7×10^6										
		2.8×10^6			Sting				Yes			
		3.7×10^6										
		4.5×10^6										
		3.7×10^6	3.0				Yes					
		3.7×10^6	6.0									
		2.8×10^6	0			Yes						
		3.7×10^6										
		4.5×10^6										
		3.7×10^6	3.0									
		3.7×10^6	6.0									
	1.40	3.8×10^6	0			No						
		3.8×10^6				Yes						
Flat		3.8×10^6				No	No		Rear forebody			
		3.8×10^6				Yes						
	1.59	1.8×10^6			Wire	No	Yes	No	No			
		2.7×10^6										
		3.7×10^6										
		4.7×10^6										
Recessed		1.8×10^6										
		2.8×10^6										
		3.7×10^6						Yes				
		4.7×10^6						No				
Rocket		2.7×10^6										
		3.7×10^6										
		4.7×10^6										
		3.7×10^6			Sting			Yes				

NACA

Security Classification of This Report Has Been Cancelled

TABLE II.- SUMMARY OF BASIC TEST PROGRAM CONDUCTED ON RM-10 FORCE MODEL - Concluded

Base configuration	M	R	ε	Number of fins	Method of support	Transition strip at $\frac{x}{l}=0.615$	Drag force data	Base pressure measured	Pressure-distribution tests	Nose configuration	Nose location in tunnel (see fig. 3)	Internal air flow through model
Rocket	1.40	3.8×10^6	0	1	Sting	No	Yes	Yes	No	Faired	215	Yes
	1.59	2.7×10^6		(180° 2 apart)	Wire			No				
		3.7×10^6										
		4.7×10^6										
		3.7×10^6			Sting			Yes				
	1.40	3.8×10^6		(90° 2 apart)								
		3.8×10^6				Yes						
	1.59	1.8×10^6		(90° 3 apart)	Wire			No				
		2.7×10^6										
		3.7×10^6										
		4.7×10^6										
		2.7×10^6		(120° 3 apart)		No						
		1.9×10^6		4								
		2.7×10^6										
		3.7×10^6										
		4.7×10^6										
		2.8×10^6			Sting			Yes				
		3.7×10^6										
		4.5×10^6										
		2.8×10^6				Yes						
		3.7×10^6										
		4.5×10^6										
	1.40	3.8×10^6				No						
		3.8×10^6				Yes						
Flat	1.59	2.7×10^6		(120° 3 apart)	Wire	No		No				
		3.7×10^6										
		4.7×10^6										
		2.7×10^6		4								
		3.7×10^6										
		4.7×10^6										
	1.40	3.8×10^6			Sting		No	Yes	Rear forebody			
		3.8×10^6				Yes						
Recessed	1.59	2.7×10^6			Wire	No	Yes	No	No			
		3.7×10^6										
		4.7×10^6										

TABLE III.- TABULATION OF DIFFERENCE BETWEEN COMPUTED AND

MEASURED ORDINATES FOR RM-10 FUSELAGE
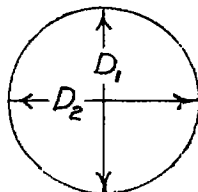
Fore part of body			Rocket base		
x	$D_{computed} - D_1$	$D_{computed} - D_2$	x	$D_{computed} - D_1$	$D_{computed} - D_2$
3.05	0.004	0.001	34.05	0.006	0.008
4.05	-.004	-.004	35.05	0	.006
5.05	.002	.001	36.05	-.003	0
6.05	-.001	-.001	37.05	-.005	-.003
7.05	-.007	-.007	38.05	-.002	0
8.05	-.009	-.009	39.05	.001	.002
9.05	-.011	-.011	40.05	.004	.005
10.05	-.011	-.013	41.05	.007	.007
11.05	-.012	-.013	42.05	.005	.004
12.05	-.011	-.011	Recessed base		
13.05	-.010	-.010	34.05	0.007	0.007
14.05	-.010	-.011	35.05	.003	.004
15.05	-.010	-.013	36.05	0	0
16.05	-.011	-.014	37.05	-.005	-.006
17.05	-.008	-.010	38.05	-.003	-.004
18.05	-.004	-.006	39.05	-.001	-.003
19.05	-.005	-.004	40.05	.002	0
20.05	-.002	-.003	41.05	.001	-.001
21.05	0	0	42.05	.002	.002
22.05	0	-.001	Flat base		
23.05	-.001	0	34.05	0.009	0.008
24.05	.003	.002	35.05	.002	.003
25.05	.004	.005	36.05	-.002	-.002
26.05	.006	.006	37.05	-.006	-.007
27.05	.006	.007	38.05	-.005	-.006
28.05	.004	.006	39.05	0	-.002
29.05	.003	.005	40.05	.001	0
30.05	.003	.003	41.05	-.004	-.006
31.05	.003	.002	42.05	-.009	-.010
32.05	-.001	-.002			
33.05	.001	0			
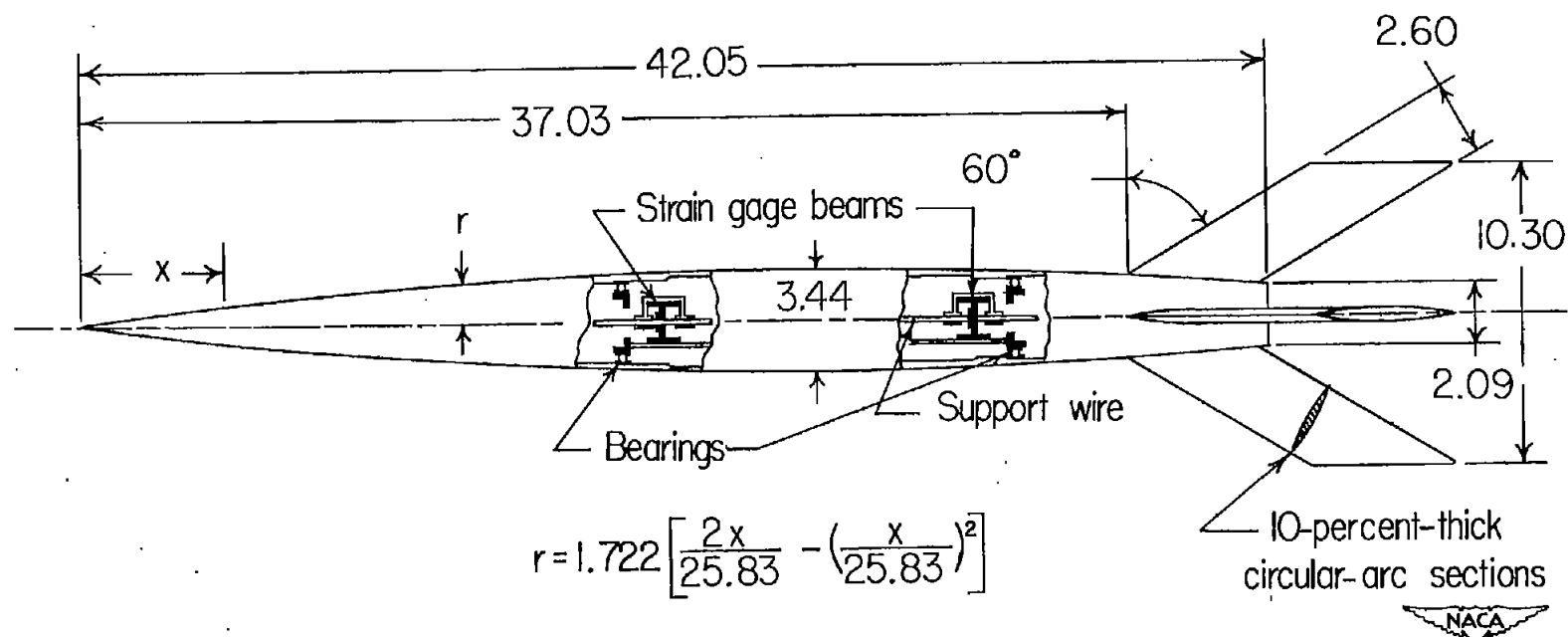
Figure 1.- Drawing of 0.287-scale model of RM-10. All dimensions are in inches.

x'	r'
0	.915
.861	.507
1.148	.408
1.722	.516
1.937	.762

a. Faired nose detail.

b. Rocket base.

c. Recessed base.

d. Flat base.

e. Pointed base.
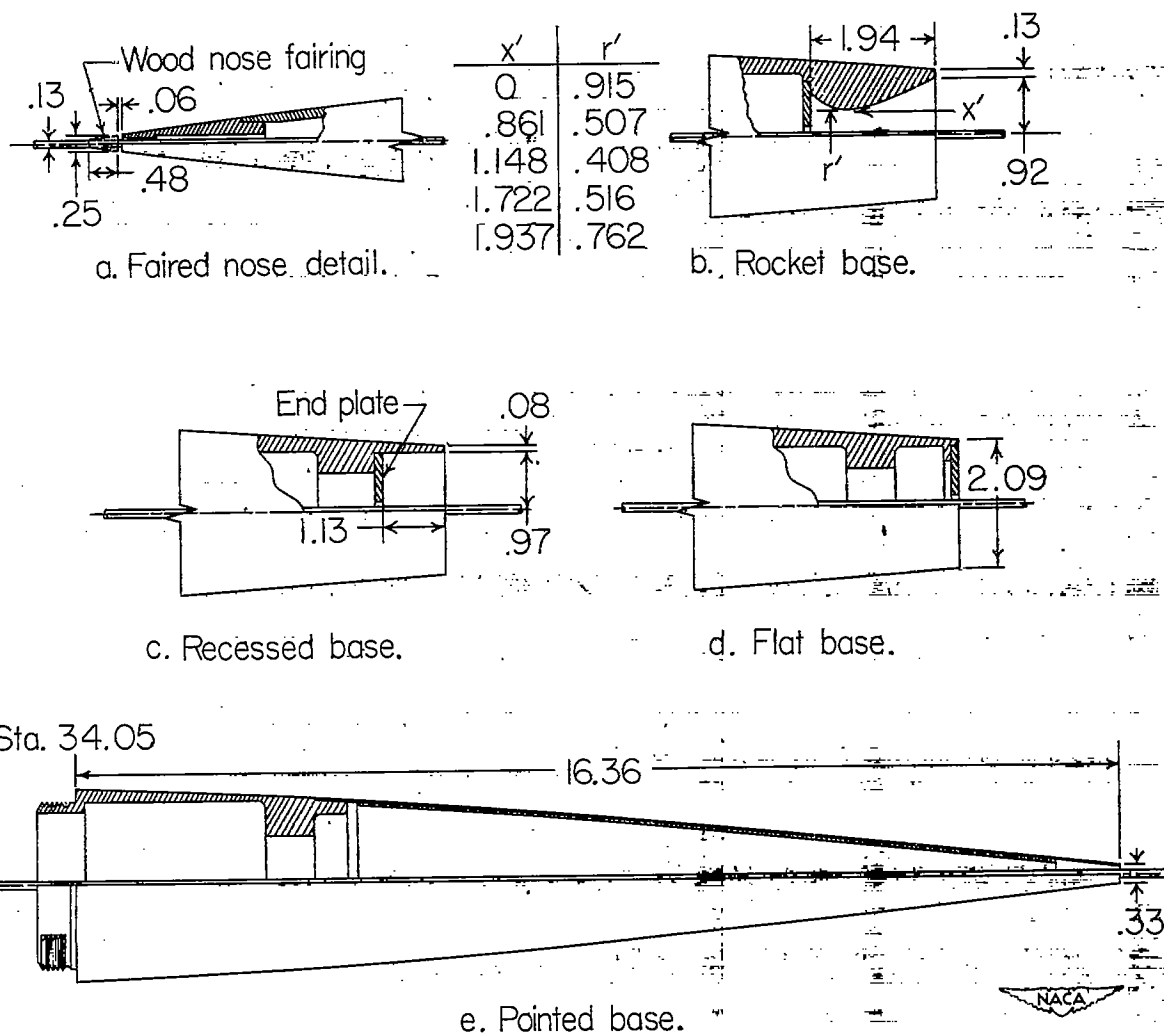
Figure 2.- Nose and base details of wire-supported model. All dimensions are in inches.
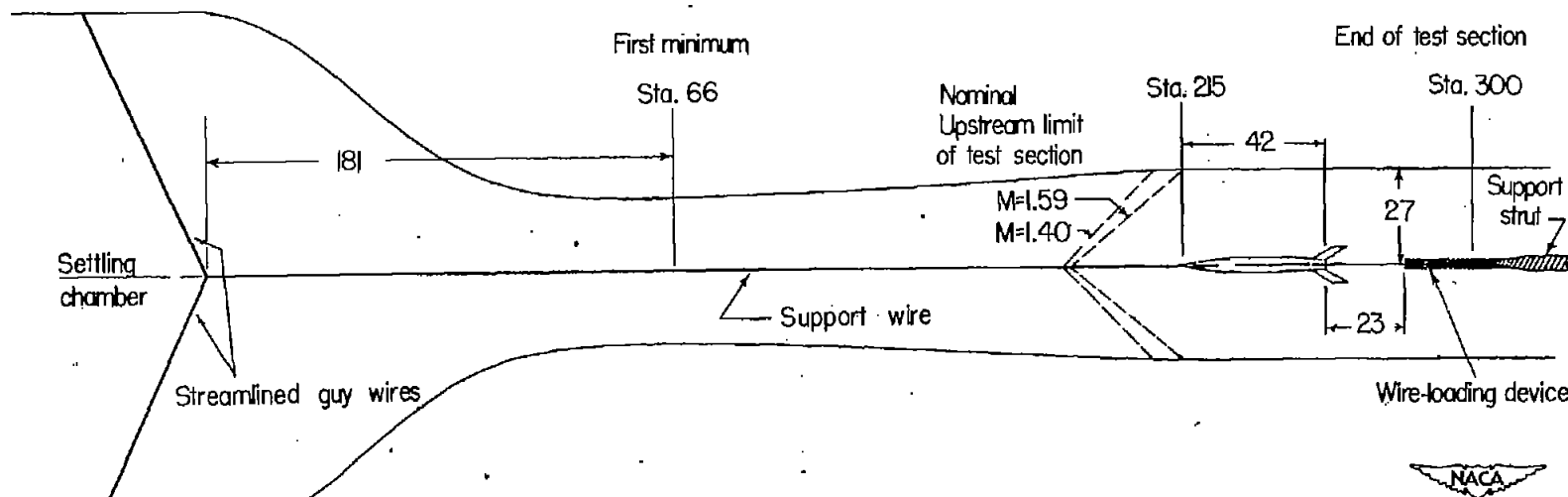
Figure 3.- Test setup for wire-supported model. All dimensions are in inches.
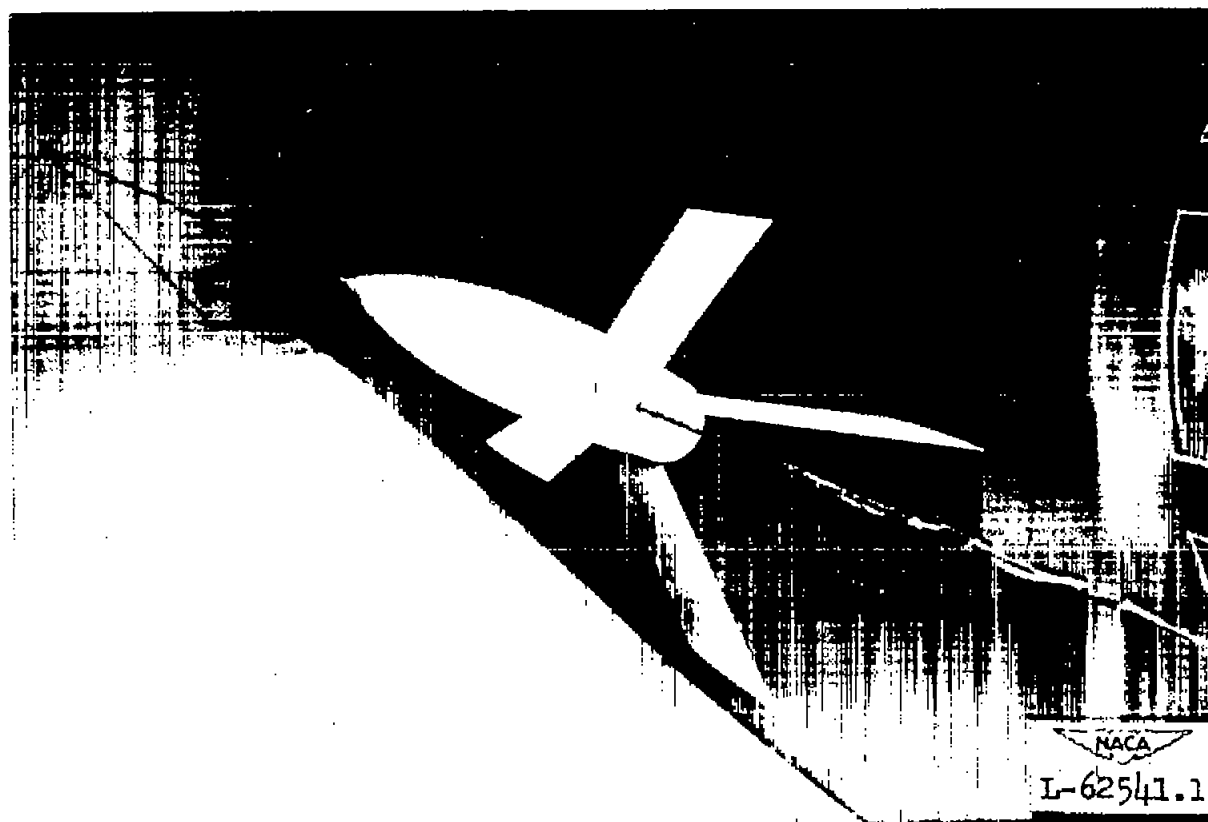
Figure 4.- Photograph of wire-supported model.

L-63985
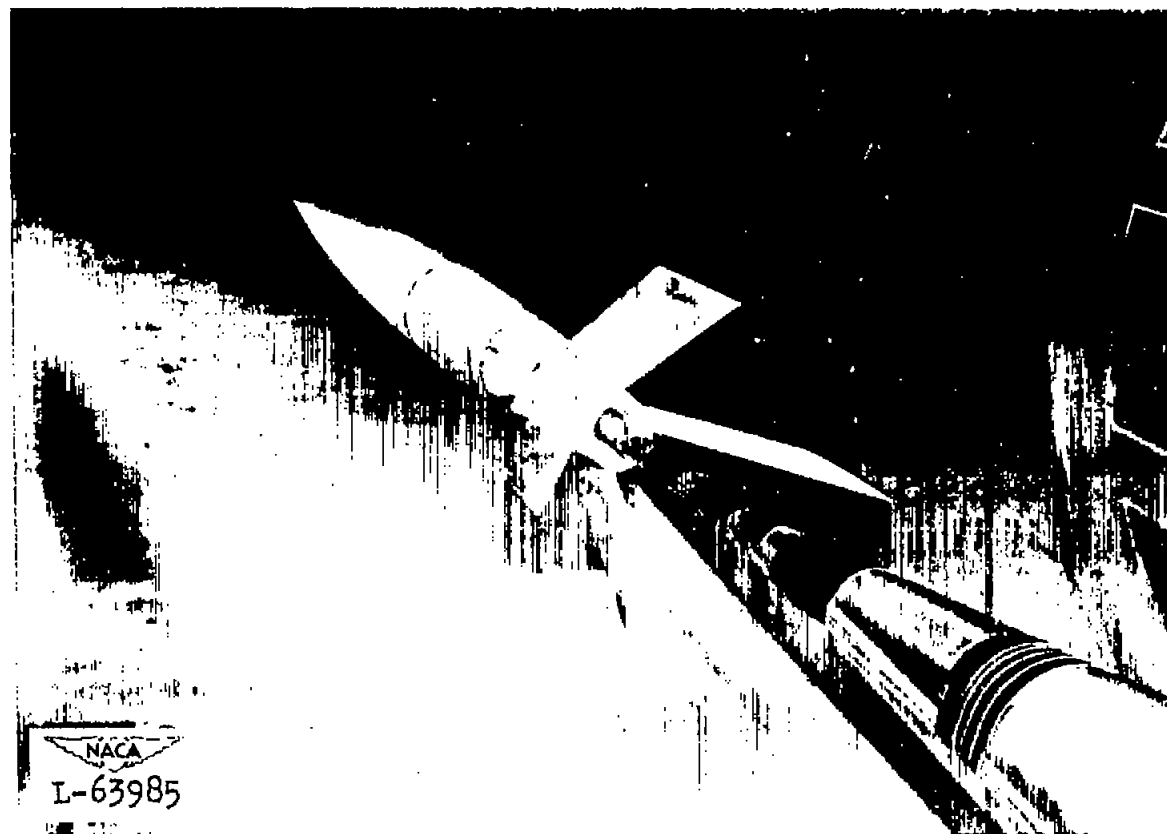
Figure 5.- Photograph of sting-supported model.
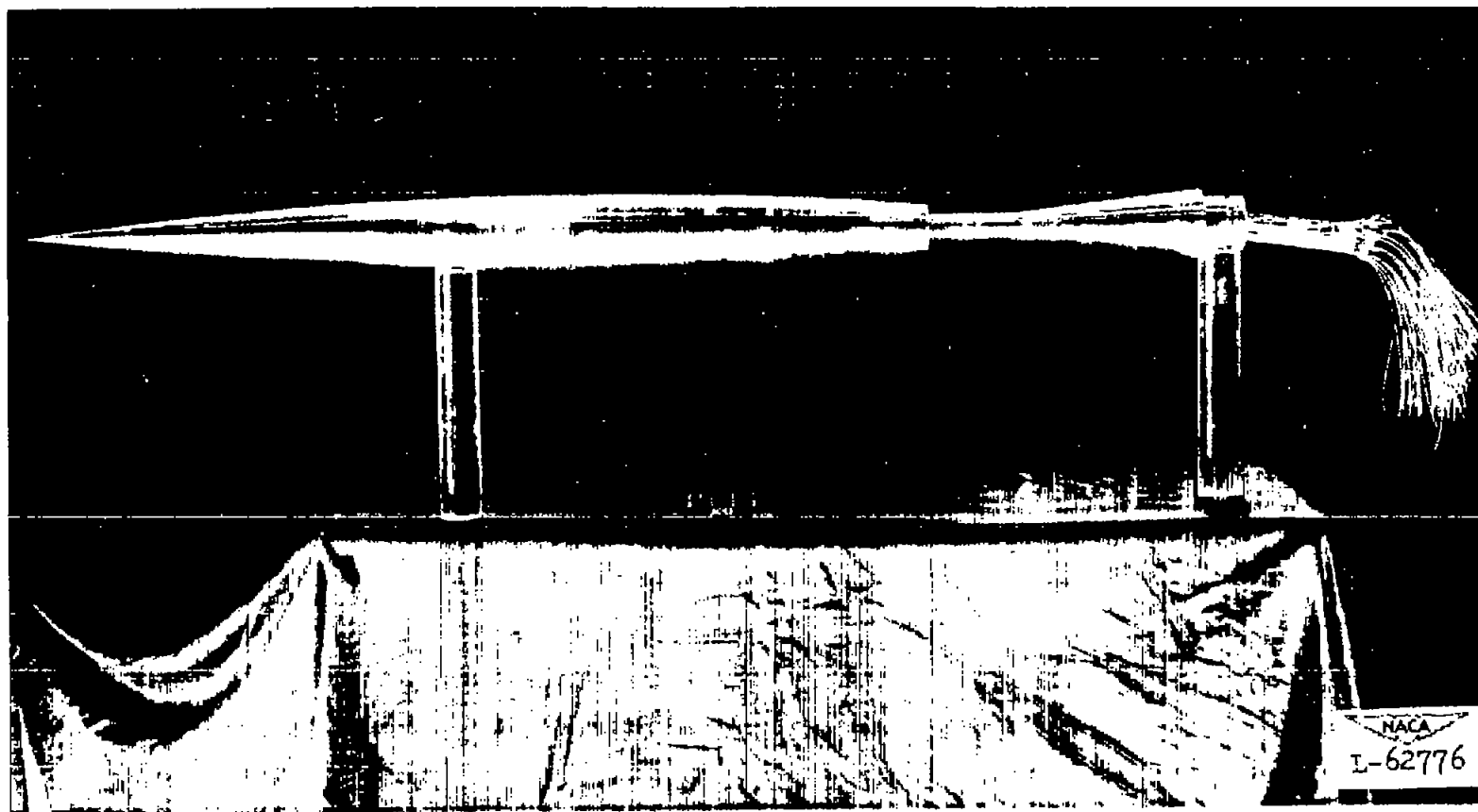
Figure 6.- Photograph of pressure model.
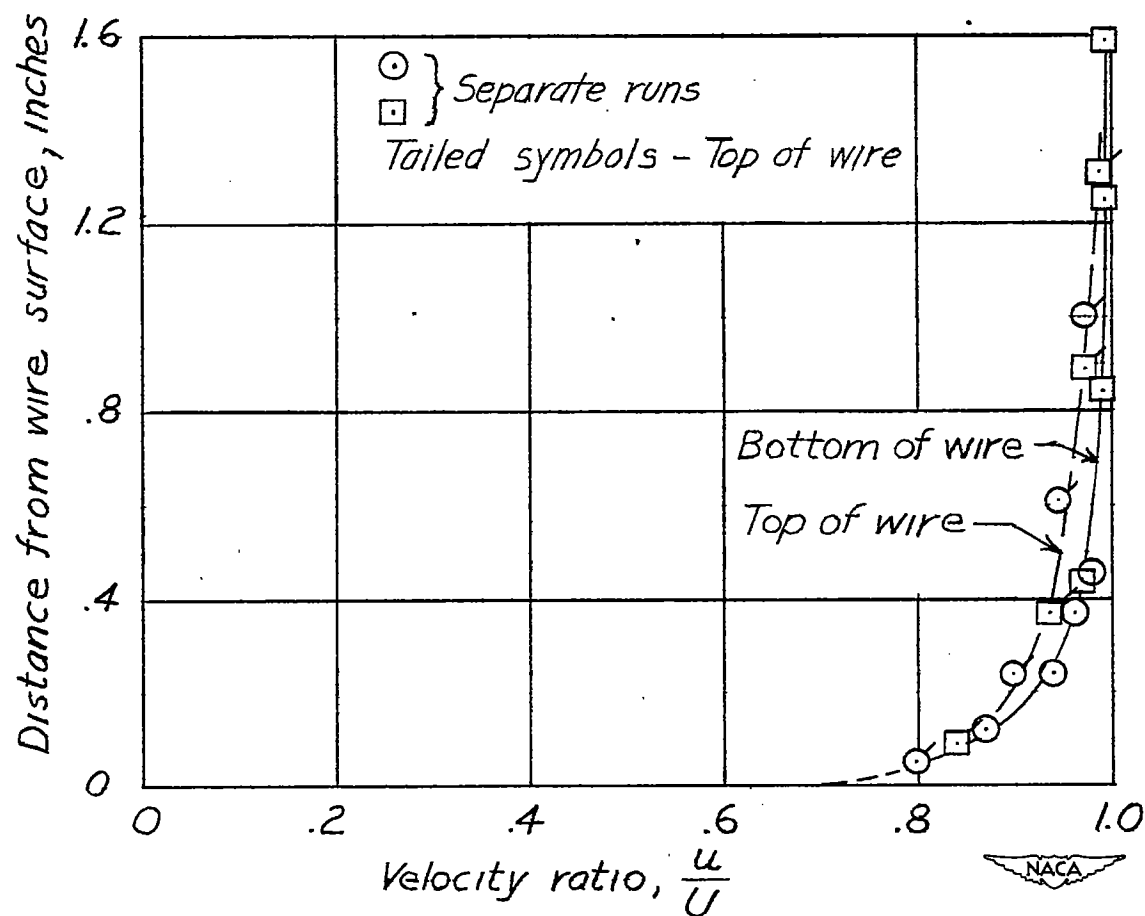
Figure 7.- Wire boundary-layer profiles measured at nose of model: M = 1.59; R = 3.7 × 10^6 based on model length.
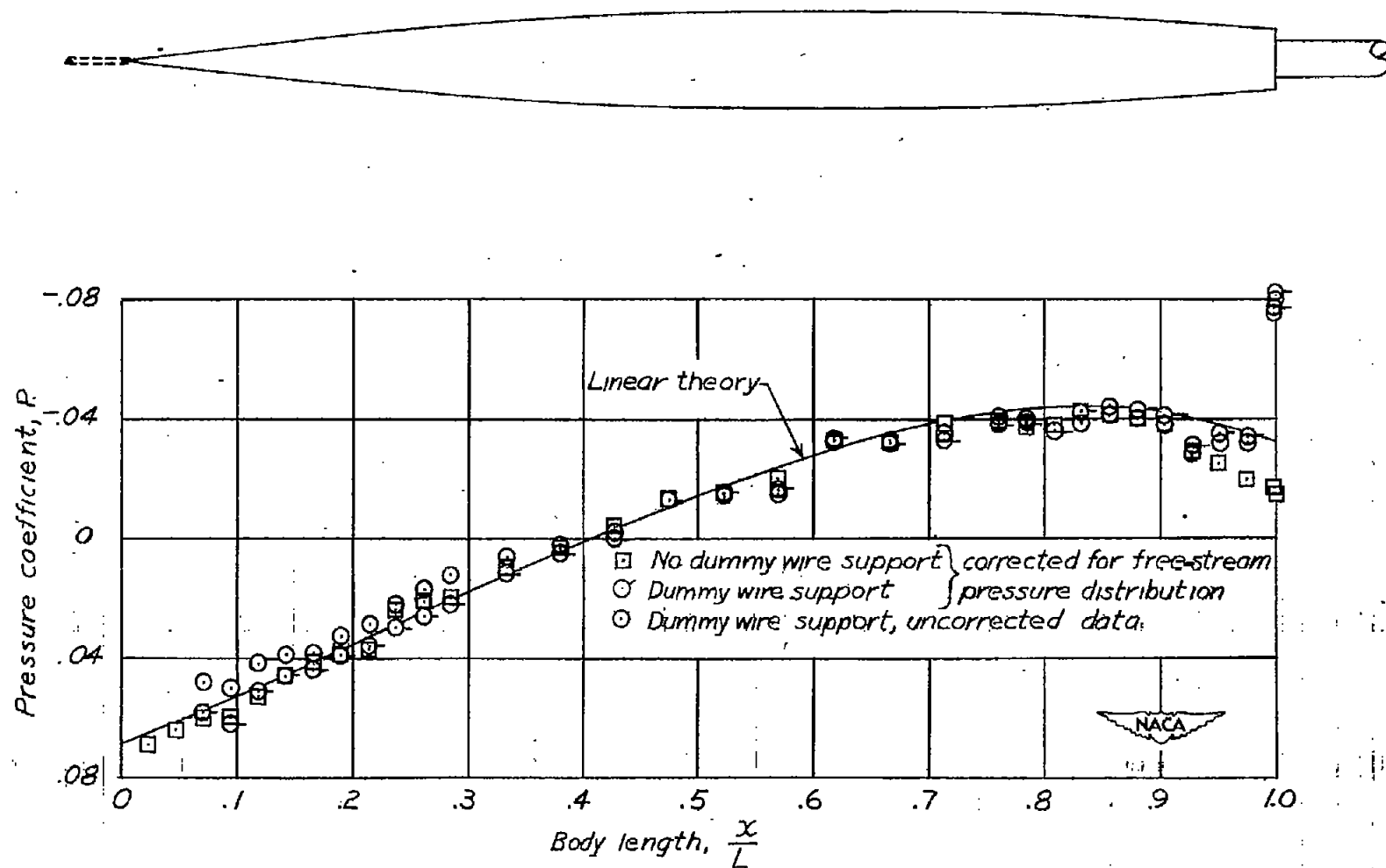
Figure 8.- Pressure distribution obtained on pressure model with and without the dummy wire support. M = 1.59; R = 3.7 × 10⁶.
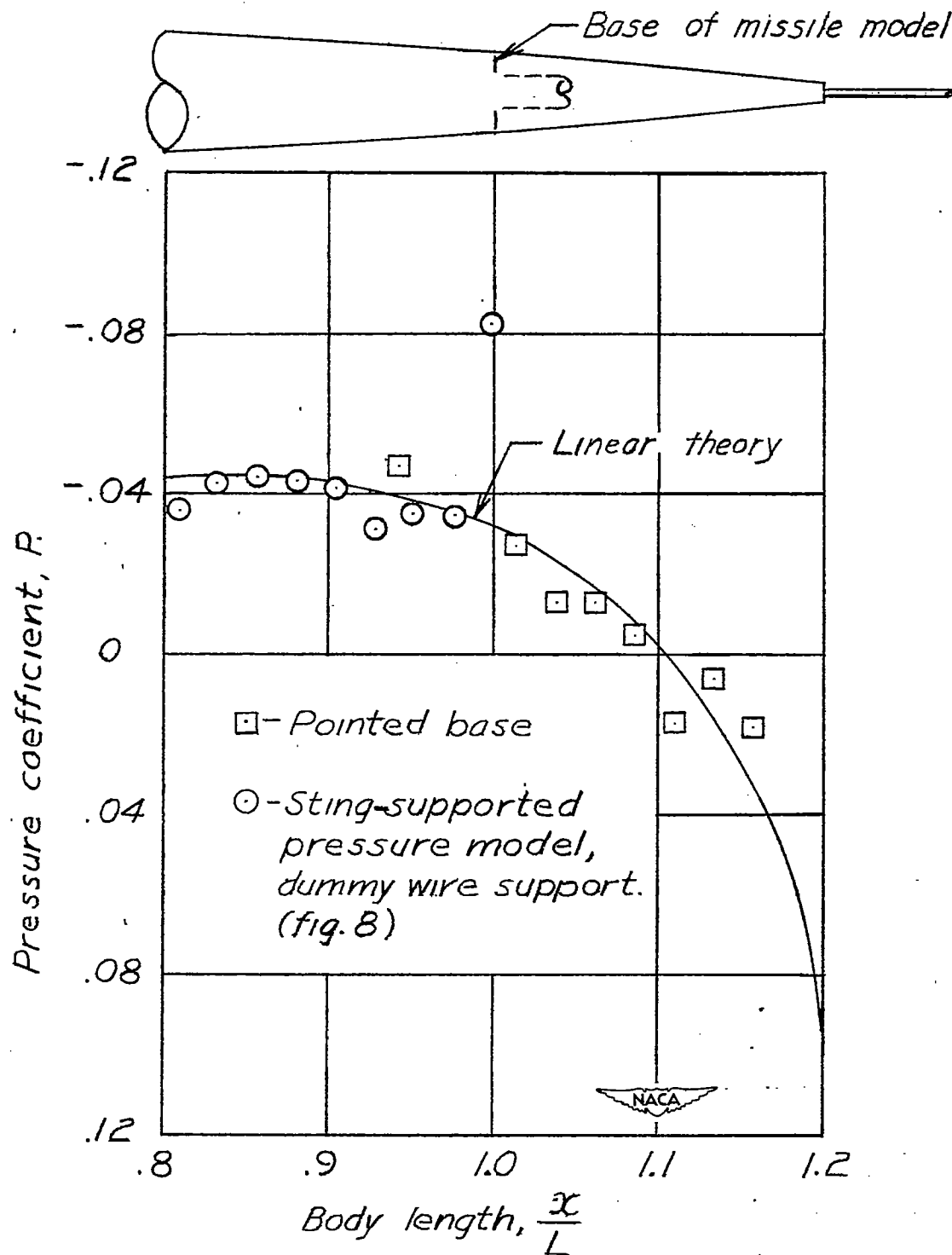
Figure 9.- Pressure distribution over pointed base model. M = 1.59;
R = 3.7 × 10^6.
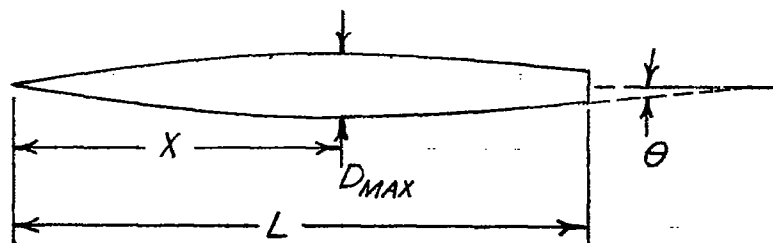
	$\dfrac{X}{L}$	$\dfrac{L}{D_{MAX}}$	θ	M	R
Model 4	.567	8.82	8.55	1.5	3.70×10^6
Model 5	.567	6.18	12.13	1.5	3.70×10^6
RM-10	.614	12.20	4.80	1.59	3.70×10^6

⊙ Ames 1x3-foot data (Reference 10)

☐ Langley 4 x 4-foot data

Tailed symbols represent turbulent flow
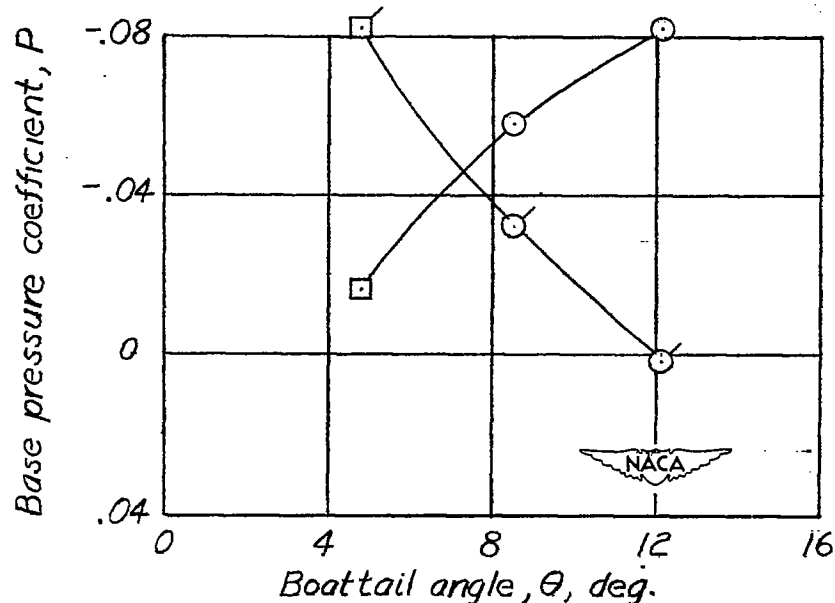
Figure 10.- Variation of base pressure coefficient with model boattail angle for laminar and turbulent boundary-layer flow over the rear of three parabolic bodies of revolution.
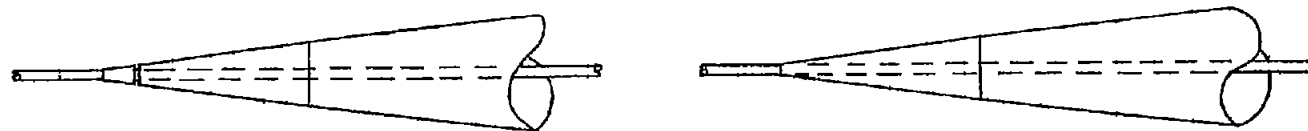
Wire -supported model

$\emptyset$
(degrees)

0	180	
⊙	▫	Flow through model
⊙	▱	No flow through model

Sting -supported pressure model

◇ Average pressure from four orifices with equal radial spacing.
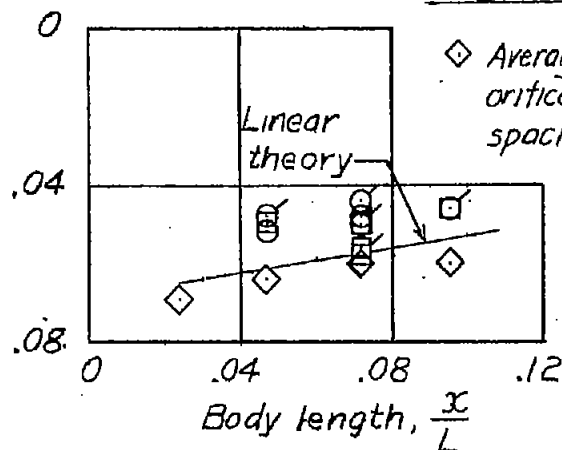
(a) Faired nose.
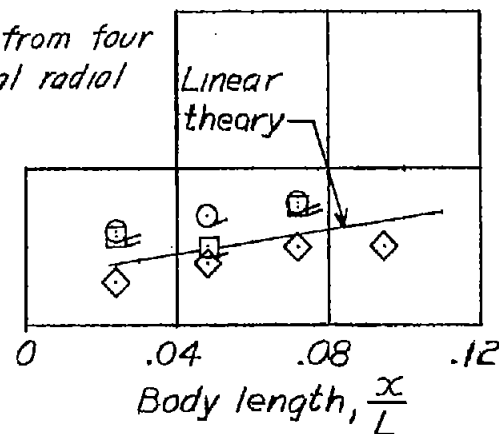
(b) Tight fitting nose.

Figure 11.- Effect of wire support on nose pressure distribution.
$M = 1.59$; $R = 3.7 \times 10^6$.
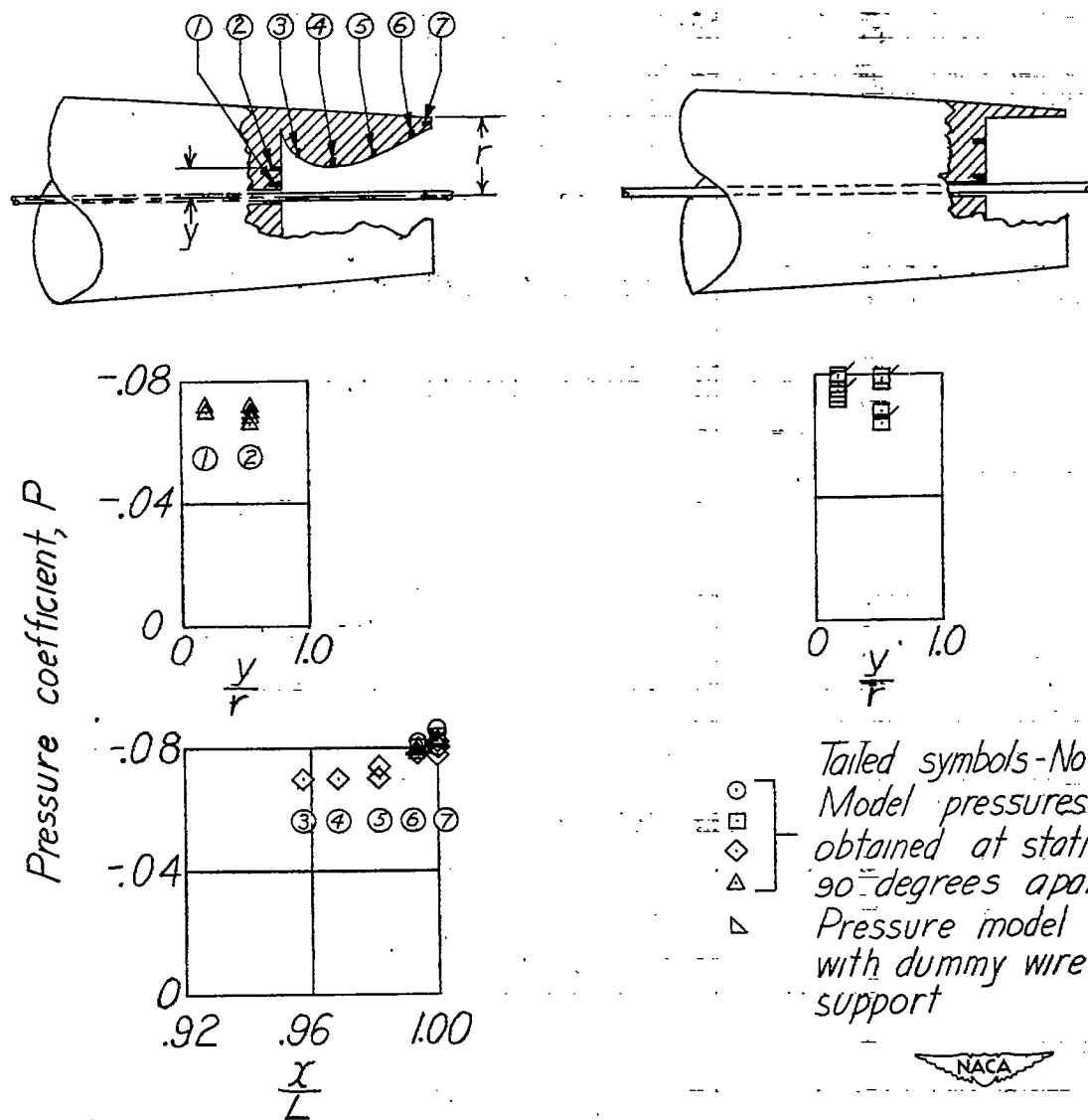
Figure 12.- Effect of wire support on base pressure distribution.
M = 1.59; R = 3.7 × 10^6.
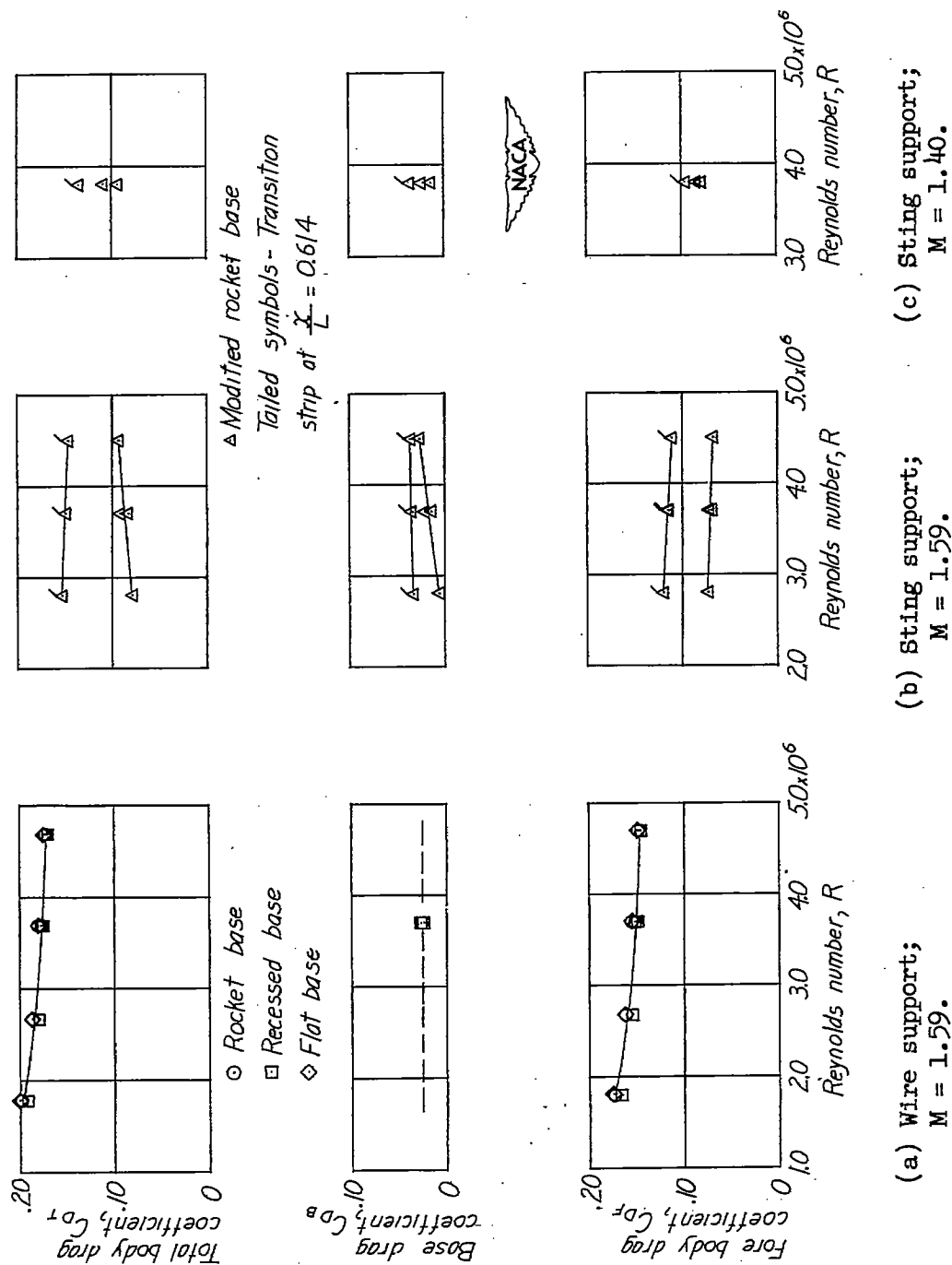
Figure 13.- Variation with Reynolds number of the drag characteristics of the wire- and sting-supported force model (body alone) at an angle of attack of 0°.

(a) Wire support; M = 1.59.

(b) Sting support; M = 1.59.

(c) Sting support; M = 1.40.

CONFIDENTIAL

Computed skin friction drag coefficients

————————— Complete laminar (Equation 2)

———————— Complete turbulent (Equation 3)

—— —— —— Transition strip at $\frac{x}{L}=0.614$

⊙   Rocket base
▣   Recessed base } Wire support
◇   Flat base

△   Rocket base — Sting support
Tailed symbols — Transition strip at $\frac{x}{L}=0.614$
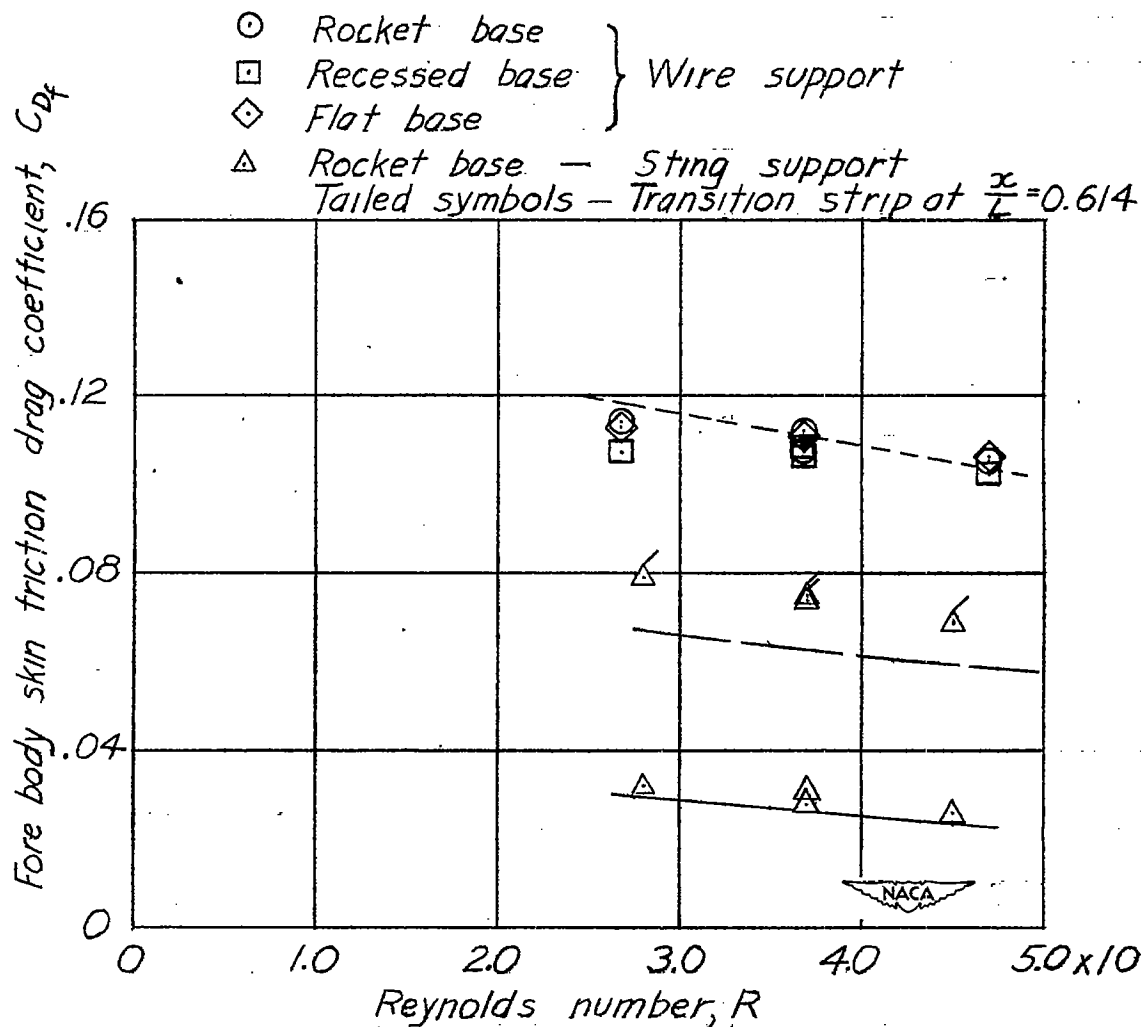
Figure 14.- Variation with Reynolds number of the forebody skin-friction coefficient of the wire- and sting-supported models (body alone). M = 1.59.

CONFIDENTIAL
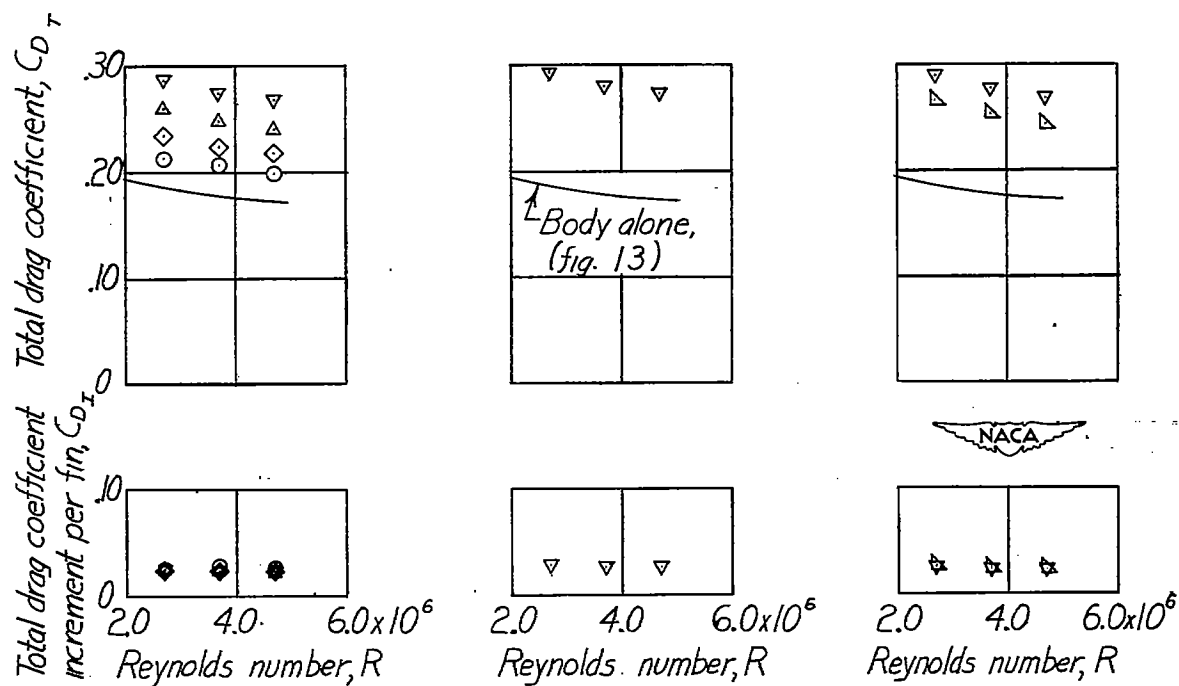
CONFIDENTIAL

(a) Rocket base.   (b) Recessed   (c) Flat base.
                              flat plate.

Figure 15.- Drag characteristics of wire-supported complete model.
M = 1.59; α = 0°.

CONFIDENTIAL
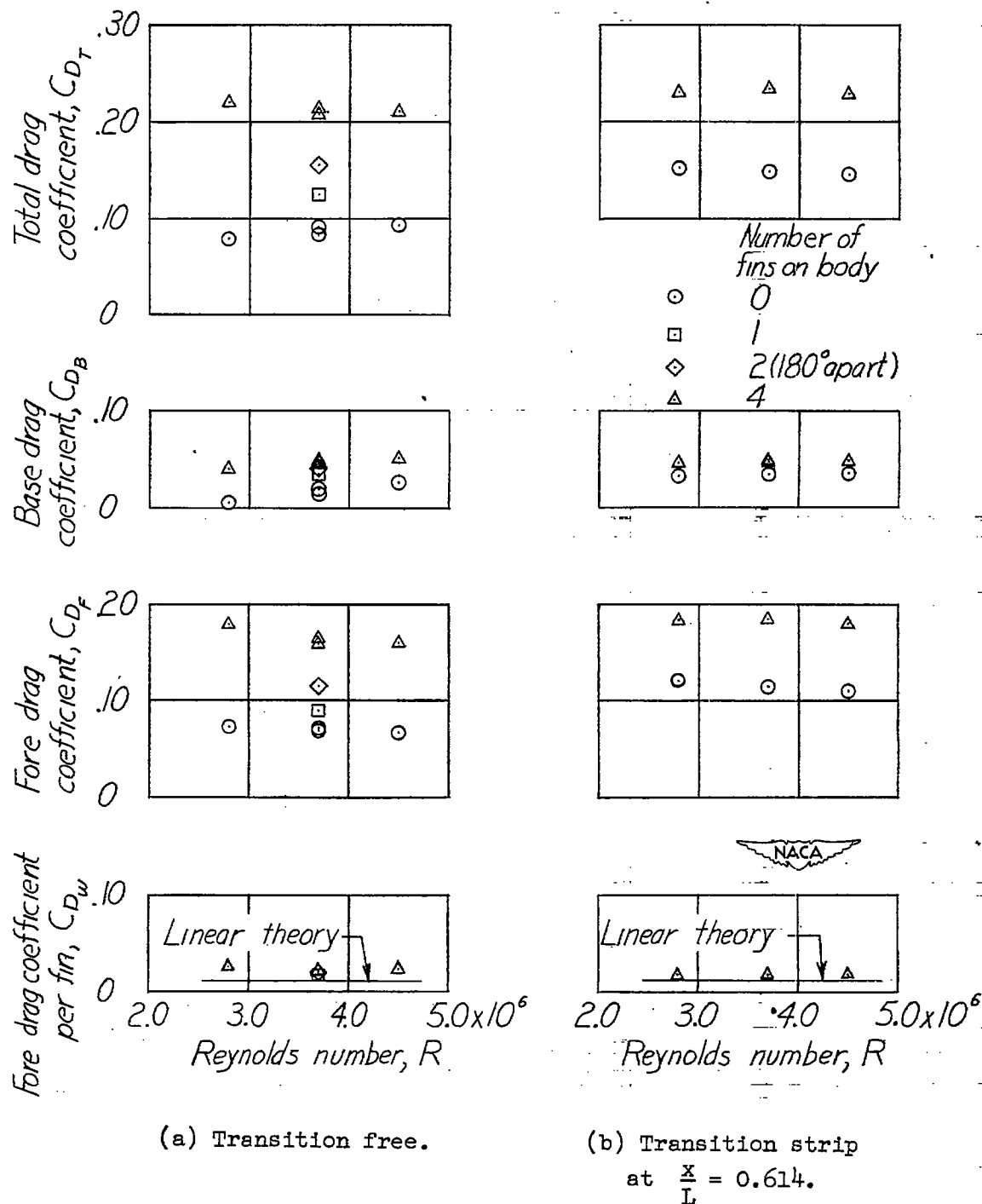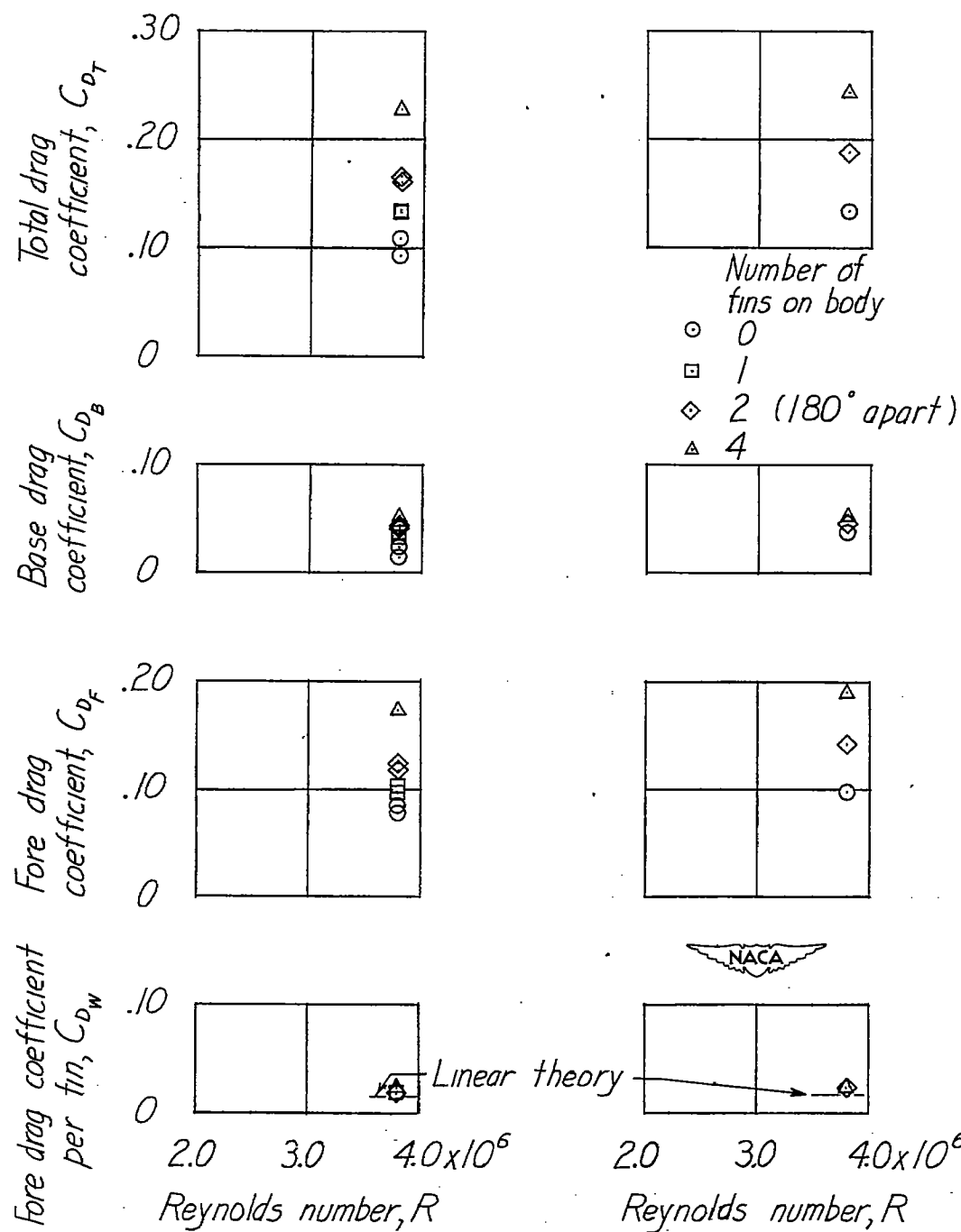
(a) Transition free.

(b) Transition strip at $\frac{x}{L} = 0.614$.

Figure 16.- Variation with Reynolds number of the drag characteristics of the sting-supported model with and without fins. M = 1.59; α = 0°.

(a) Transition free.

(b) Transition strip
at $\frac{x}{L} = 0.614$.

Figure 17.- Variation with Reynolds number of the drag characteristics
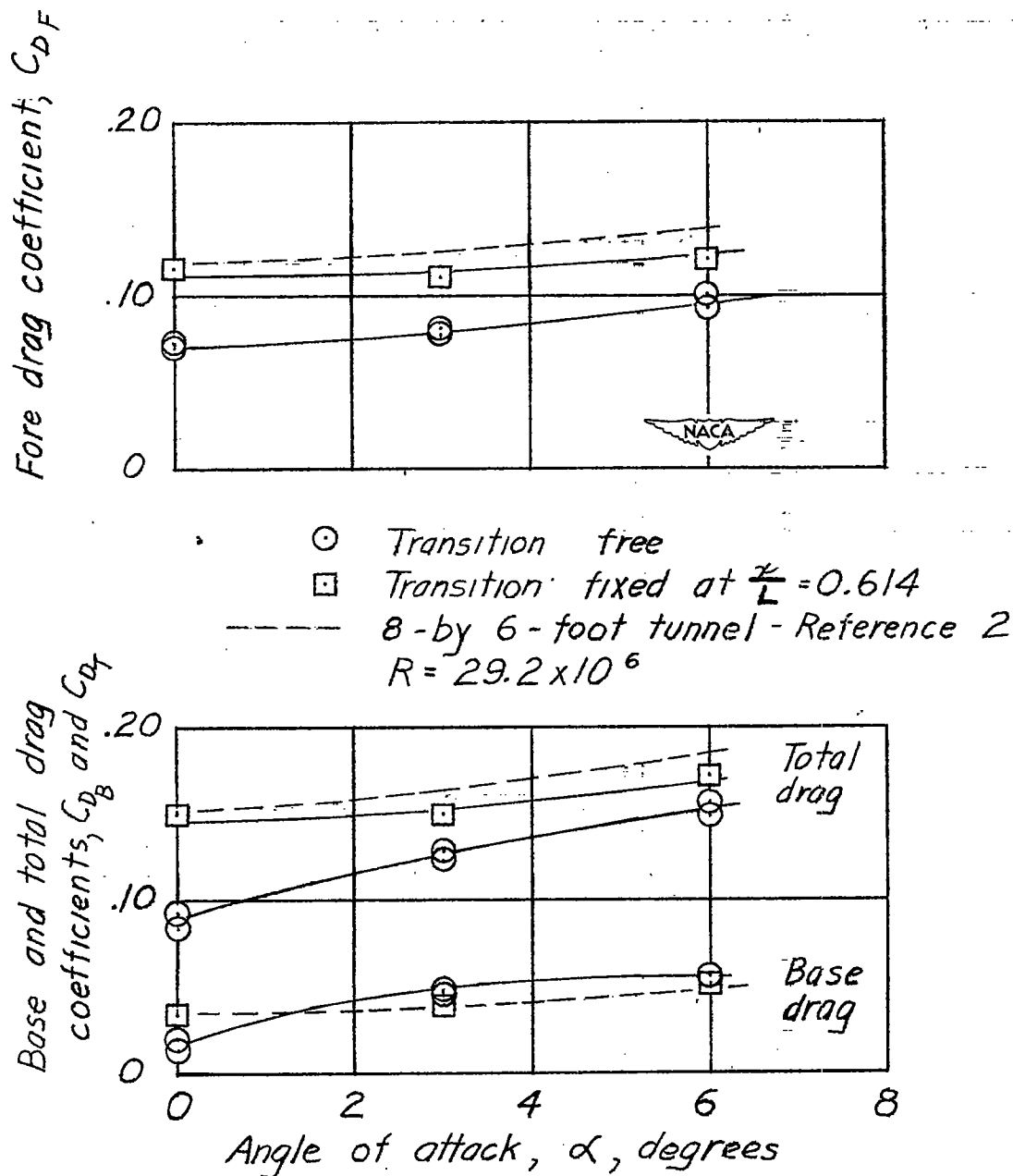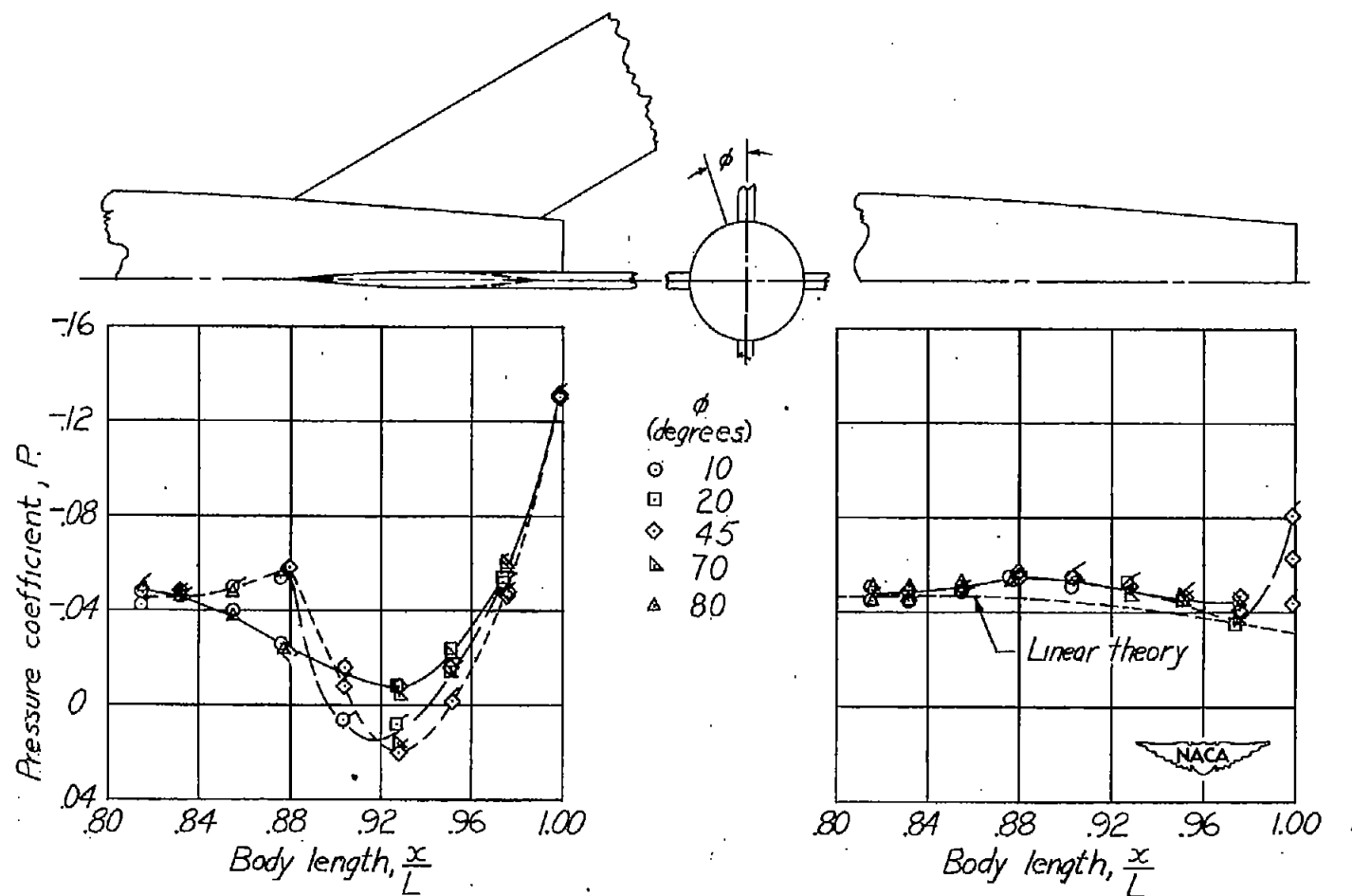of the sting-supported model with and without fins. M = 1.40; $\alpha = 0°$.

CONFIDENTIAL

Figure 18.- Variation with angle of attack of the drag characteristics of the body alone. $M = 1.59$; $R = 3.7 \times 10^6$.

(a) Complete model.

(b) Body alone.

Figure 19.- Effect of fins on fuselage pressure distribution for laminar and turbulent boundary layer flow. $M = 1.40$; $R = 3.8 \times 10^6$. Tailed symbols indicate fixed transition.

CONFIDENTIAL

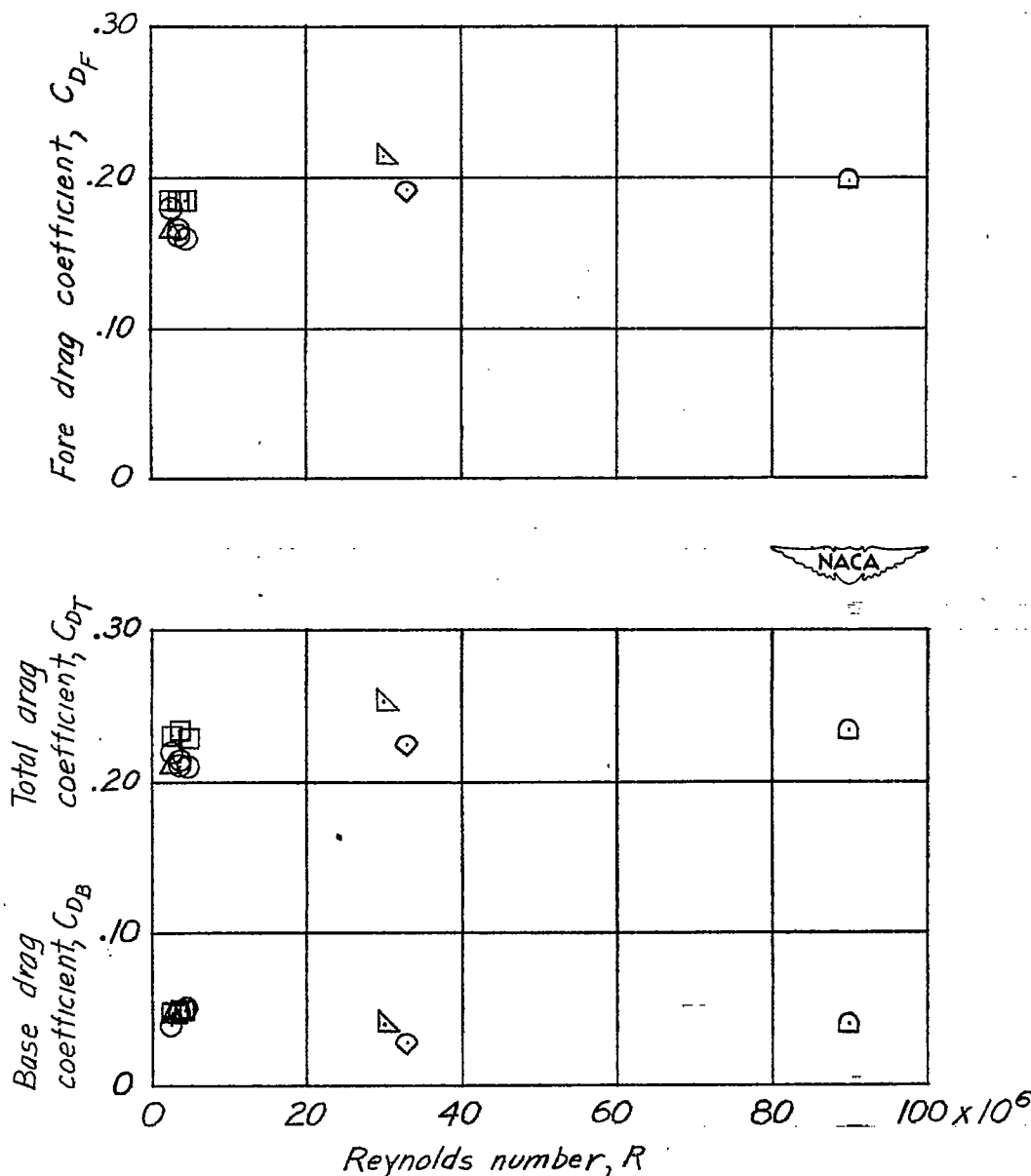|		$D_s/D_{max.}$		M
⊙	4-by 4-foot tunnel	0.208	Transition free	1.59
⊡	4-by 4-foot tunnel	0.208	With transition strip	1.59
△	9 inch tunnel	0.297	Unpublished data	1.62
◁	8-by 6-foot tunnel	0.400	Reference 2	1.59
⌂	PARD - Full scale		Reference 5	1.59
◇	PARD - Half scale		Reference 5	1.59

Figure 20.- Variation of the drag characteristics of the complete model over a large Reynolds number range near a Mach number of 1.6. α = 0°.

CONFIDENTIAL

			M
△	9 inch tunnel	Unpublished data	1.62
◇	PARD - Half scale }	Reference 5	1.59
◙	PARD - Full scale }		
⊙	4-by 4-foot tunnel	Transition free	1.59
⊡	4-by 4- foot tunnel	With transition strip	1.59
◮	4-by 4 -foot tunnel	Wire supported model	1.59
◺	8-by 6-foot tunnel	Reference 2	1.59

Turbulent flow (Equation 3)

Laminar flow (Equation 2)

Forebody skin friction drag coefficient, C_{D_f}
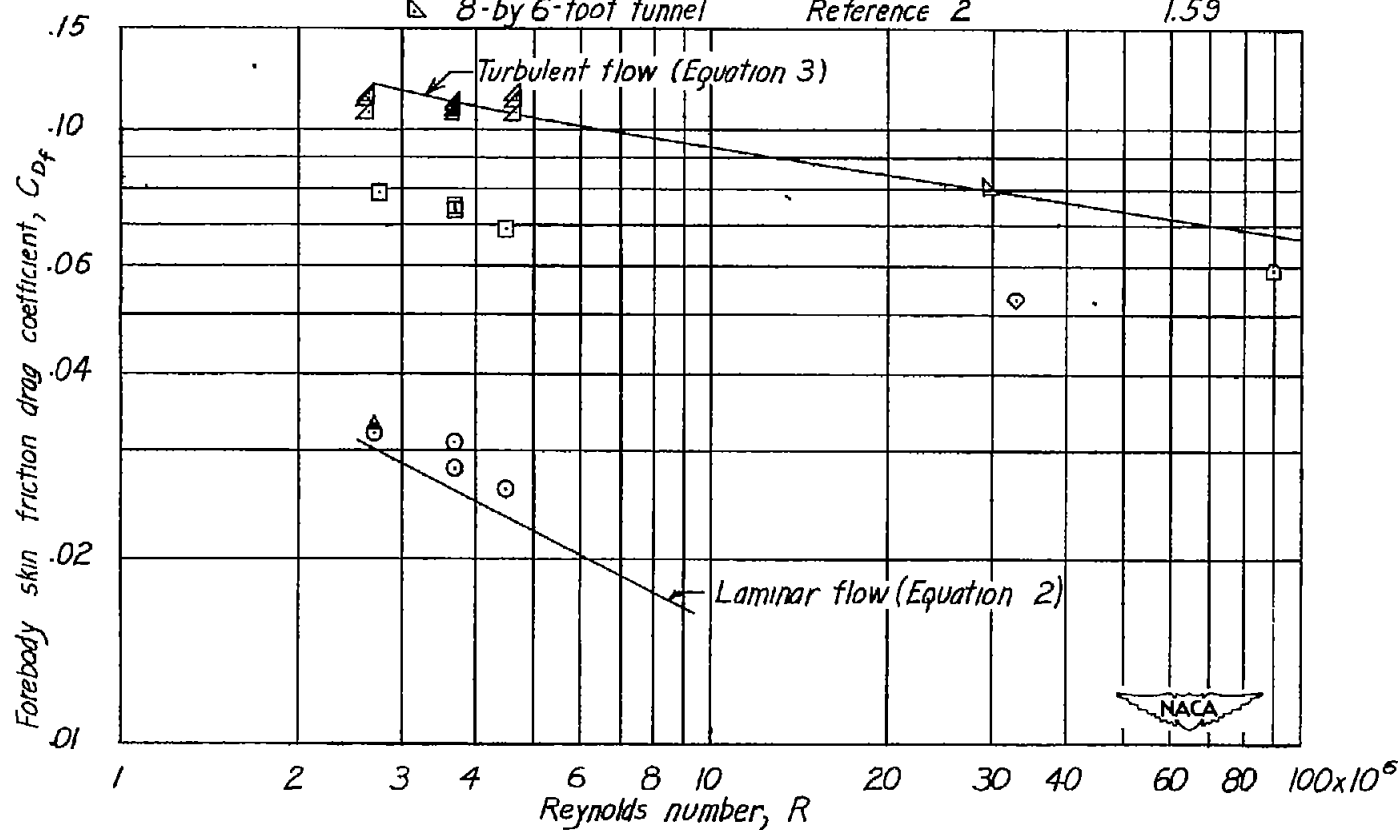
Reynolds number, R

Figure 21.- Variation of forebody skin-friction drag coefficient over a large Reynolds number range near a Mach number of 1.6. $\alpha = 0°$.